Use of 4,4'-diamino diphenyl ether to derive a novel series of diamines and their metallomacrocyclic dithiocarbamate complexes: Synthesis, characterization, DFT and cytotoxic study against Hep G2 cancer cell line

Abstract

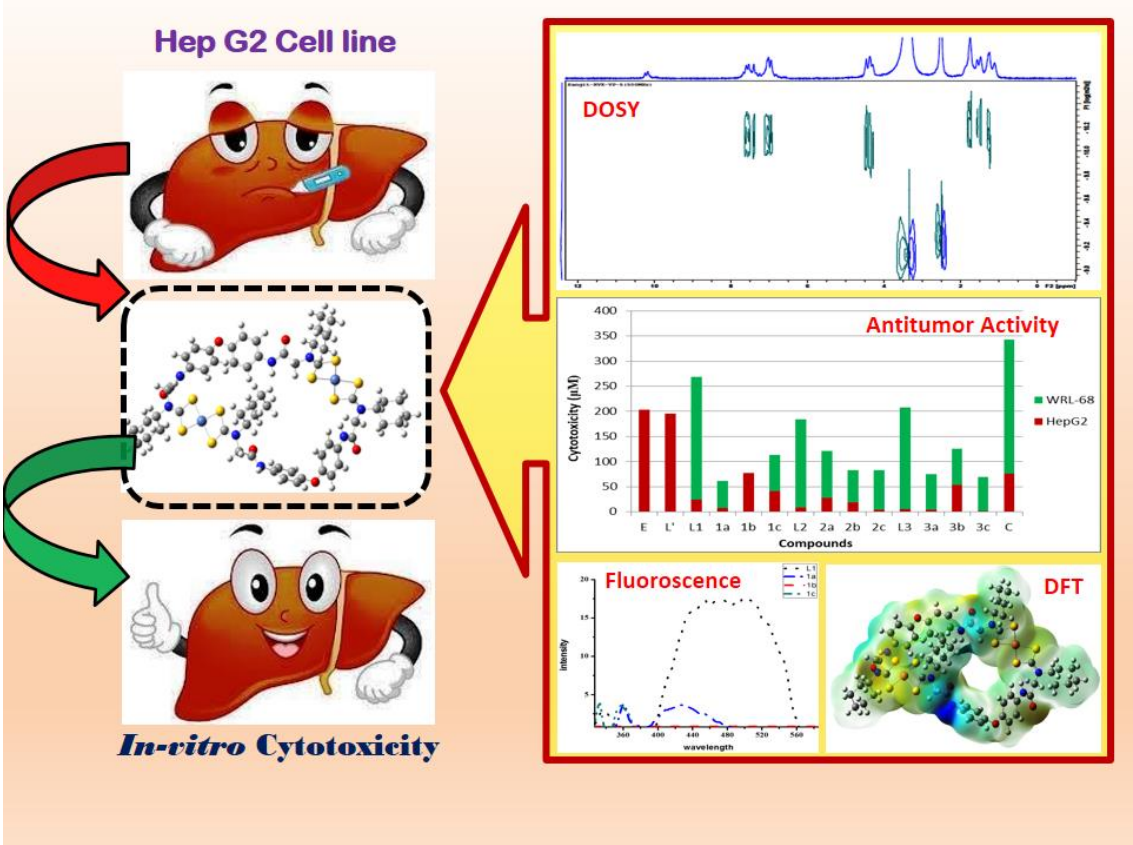

Three diamino precursors 4,4'-bis(2-(alkylamino)acetamido)diphenylether (**L^1-L^3**) of a 4, 4'- oxydianilne was selected to derive new series of metallomacrocyclic-dtc complexes and their potential to be substantial cytotoxic agents against Hep G2 cell line, their specificity for cancer cells over normal liver cells were investigated. Assembly of

number of pharmacophores on a single molecular platform evidently lead to improved therapeutic efficiencies and reduced side effects of conventional chemotherapy drugs. The acridine orange/ethidium bromide (AO/EB) staining and morphological investigations clearly indicate the induction of apoptotic cell death.

5.1 Introduction

4,4'- oxydianilne commonly abbreviated as ODA has been efficaciously used since a long time in the field of material chemistry for development of promising materials for membranes owing to their properties of excellent permselectivity and stability in the form of organic glassy polymers like polyimides.[1-7] The derivatives of ODA displayed excellent thermal stability[8] and increased membrane permeability [4] due to the introduction of a rigid and bulky dianiline structure with inhibited rotation around –O– linkages. Further reports suggests that presence of 4,4'- oxydianilne in Pyromellitic dianhydride-4,4' -oxydianiline (PMDA-ODA) polyimide improved its mechanical stability and lowered the dielectric constant as well as improved the chemical resistance and thus became important for many advanced technologies in the electronic industry.[9] Besides biological perspective of 4,4'- oxydianilne suggests that the presence of it in the diet of male and female F344 rats incidences adenomas of the thyroid gland, neoplastic nodules and harderian gland, noticeably,[10] however tumour-inhibiting property of 4,4'-oxydianiline in mice is also highlighted in the literature.[11] The pharmacokinetic study 4,4'-oxydianiline to rats reveals that ~16 % of the dose was recovered in the urine within 72 hours as the unchanged substance and the metabolites, N-acetyl-4,4'-oxydianiline and N,N'-di-acetyl-4,4'-oxydianiline.[12] While a primary investigation on in-vivo mutagenicity of 4,4'-oxydianiline and its N-acetyl derivative towards Salmonella typhimurium TA98 and TA100 was reported in 1985 by Tanaka et al.[12], we have solely explored the cytotoxic activity of some of the derivative of 4,4'-oxydianiline on human HEP 3B and IMR 32 cell lines, recently.[13-14]

In the light of a high degree of potency and selectivity shown by a wide range of natural products bearing macrocyclic motifs [15-17] in medicinal chemistry, synthetic chemists are

enthused to discover a broader use of macrocyclic frameworks in therapeutic uses. In recent times, our lab has examined in vitro cytotoxic activity of a number of 1,1-dithio based metallomacrocyclic complexes and some of these complexes evidently showed remarkable activity against human hepatoma and neuroblastoma cell lines.[14,18-19] The sulfur atoms in molecule as donor sites reportedly play various role viz. as chemoprotectants in platinum-based chemotherapy, to modulate cisplatin nephrotoxicity and in transporting the molecule to the targets as well as protect against untimely reaction with biomolecules.[20-23] In spite of appreciated efficacy of macrocyclic compounds and sulphur donor ligands in biological processes (*vide supra*), the metallomacrocyclic dithiocarbamates complexes are surprisingly far less studied from medicinal perspectives.[14, 18-19, 24]

In the light of these observations and encouraging cytotoxicity observed for bisimine, diamine and diphenyltin^{IV}dithiocabamate macrocyclic derivatives of 4'4'-oxydianiline against two malignant human cell lines (vide supra), it was relevant to use our recently reported ligand precursors[14] viz. 4,4'-bis(2-(cyclohexylamino)acetamido)diphenylether (**L^1**), 4,4'-bis(2-(isopropylamino)acetamido)diphenylether (**L^2**) and 4,4'-bis(2-(n-butylamino)acetamido)diphenyl ether (**L^3**) to derive a new series of metallomacrocyclic dithiocarbamate complexes of biologically relevant transition metal ions and to evaluate their possible cytotoxic abilities against human cancer cell line Hep G2 (Hepatoma). Hep G2 are commonly used as a model system for studies of liver metabolism and xenobiotics toxicity.[25]

5.2 Experimental section

5.2.1. Materials and Instrumentations

4, 4'-oxydianiline (**L**) was purchased from National Chemicals, metal acetates were purchased from Merck and chloroacetyl chloride along with used solvents such as chloroform, acetonitrile, absolute alcohol, n-hexane were purchased from Chemlab.

Solvents and reagents were of AR grade and these have been used without further purification. 4, 4'-bis(2-chloroacetamido) diphenyl ether (**L')** was synthesized by adopting a modified literature procedure. Reactions and manipulations were accomplished under an atmosphere of nitrogen. Melting points were recorded in open capillaries and these are uncorrected. Thin layer chromatography (TLC) was performed on Merck 60 F254 aluminium coated plates to monitor the progress of reaction. ESI MS were obtained on AB SCIEX 3200 Q TRAP LCMS instrument. Infrared (KBr pellets) spectra were recorded in the 4000-400 cm^{-1} range using a Perkin-Elmer FT-IR spectrometer. ^{1}H, ^{13}C, DEPT-135and DOSY NMR spectra were obtained on a Bruker AV-III 400 MHz spectrometer in DMSO-d^6 solvent and chemical shifts are reported in parts per million (ppm). UV-visible absorption spectra were recorded on a Perkin Elmer Lambda 35 UV-visible spectrophotometer. Fluorescence spectra were recorded on JASCO make spectrofluorometer model FP-6300. Thermogravimetric analysis was carried out on SII TG/DTA 6300 under flowing N_2 with a heating rate of 10 °C min^{-1}.

5.2.2. General synthetic procedure for diamine precursors 4,4'-bis(alkylamino)acetamido)biphenyl ether L^1-L^3

Synthesis of ligand precursors viz. 4,4'-bis(2-chloroacetamido)diphenylether (L') and 4,4'-bis(2-(cyclohexylamino)acetamido)biphenylether (L^1), 4,4'-bis(2-(isopropylamino)acetamido)diphenylether (L^2) and 4,4'-bis(2-(n-butylamino)acetamido)diphenylether (L^3) has been achieved by following the literature procedure[1] with slight modifications as given below:

To a clear solution of 4,4'-oxydianilne (1.0 g, 4.99 mmol) in dichloromethane Solid $NaHCO_3$ (3 eq.) was added and the reaction mixture was stirred for 45 minutes. To this stirring solution 2-chloroacetyl chloride was added carefully dropwise by using dropping funnel at 0 ˚C over a period of 1 hour and then allowed to stir at room temperature for 5-6 hours. The progress of reaction was well monitored by TLCs. The thick white precipitates was filtered over glass sintered crucible, washed with 3 × 10 mL of 5% of $NaHCO_3$, 3 × 10 mL of distilled water followed by hexane. residue was dried under high

vaccum to yield the white coloured 4,4'-bis(2-chloroacetamido)diphenyl ether (L') which was taken for the analysis.

^{1}H NMR (400 (DMSO-d6, 400 MHz) δ, ppm: 8.25 (s, 2H, CON*H*); 7.53-7.00 (d, 8*H*, Ph); 4.22 (s, 4*H*, COC*H*$_2$Cl); 1.64 (s, 2H, N*H*). FTIR (KBr disc, cm^{-1}): 3270.11s, 3142.4w, 3069.29m,2946.79w, 1692.10s, 167.03s, 1611.89m, 1556.75s, 1505.65s,1408.12s, 1336.78w, 1288.32w, 1241.82s, 1194.41w, 1162.72w, 1102.27m, 1013w, 979.70w, 881.61w, 853.80w, 833.42m, 822.84m, 787.60w, 744.61w, 700.09w, 634.30w, 560.16w, 504.83s.

An surplus amount of cyclohexyl amine (892.2 mg, 9 mmol), isopropylamine (531.9 mg, 9 mmol) or n-butylamine (658.2 mg, 9 mmol), was added to a ethanolic solution of 4,4'-bis(2-chloroacetamido) diphenylether (706.4 mg, 2 mmol). Catalytic quantity of Et_3N was added to the reaction mixture and then refluxed for a total of 8 hours. The development of the reaction was examined by TLC. The mixture was brought down to room temperature and then poured on ice. Precipitates were filtered under vacuum and washed with chilled water followed by n-hexane and diethyl ether to produce diamines **L^1-L^3** in appreciable yields.

4,4'-bis(2-(cyclohexylamino)acetamido)diphenylether (L^1): MW: 478.64, Yield: 822.1 mg, 86%. ESI-MS: 478.59 (M$^+$). FTIR (KBr disc, cm^{-1}): 3559.27w, 3270.88m, 3131.37w, 3050.92w, 2926.18s, 2851.21m, 1675.50s, 1604.36m, 1551.92m, 1530.55m, 1498.3s, 1448.02m, 1409.31m, 1371.59w, 1303.85m, 1220.42s, 1166.33w, 1129.32w, 1104.14w, 1012.97w, 962.29w, 925.16w, 832.35s, 513.47m.^{1}H NMR (400 MHz, DMSO-d_6): δ (ppm) 9.91 (s, 2H, CON*H*); 7.66-6.92 (d, 8H, *Ph*); 3.44 (s, 4H, NC*H*$_2$CO); 2.38 (m, 2H, C*H* of Cy); 2.02 (s, 2H, N*H*); 1.98-1.01 (m, 20H, C*H*$_2$ of *Cy*). ^{13}C NMR (400MHz, DMSO-d6) δ ppm: 171.38 (*C*=O); 153.01 (*C*-O), 134.65(*C*-N), 121.17, 119.13 (*Ph*); 56.72 (N*C*H$_2$CO); 50.42 (*C*H of Cy); 33.13-24.23 (*C*H$_2$ of Cy).DEPT-135 (400MHz, DMSO-d6) δ ppm: 121.16, 119.15 (*Ph*); 56.72 (*C*H of Cy); 50.41 (N*C*H$_2$CO); 33.16, 25.79, 25.05 (*C*H$_2$ of Cy).

4,4'-bis(2-(isopropylamino)acetamido)diphenylether (L^2): MW: 398.51, Yield: 660.6 mg, 83%. FTIR (KBr disc, cm^{-1}): 3582.93w, 3287.52m, 2965.22m, 1672.35s, 1606.13w, 1526.92m,1499.86s,1410.22w, 1383.13w, 1306.45w,1220.52s, 1169.04w, 1132.96w, 1104.37w, 1012.93w, 927.33w, 877.98w, 832.01w, 753.47w, 466.96vs, 438.38vs, 454.10vs, 407.47m.^{1}H NMR:(DMSO-d6, 400 MHz) : δ (ppm) 9.84 (s, 4H, CON*H*); 7.62-6.93 (d, 8H, *Ph*); 3.36 (s, 4H, NCH_2CO); 3.25 (s, 2H, C*H* of ^{i}*Pr*); 1.23 (s, br, 2H, N*H*), 1.00-0.99 (m, 12H, -CH_3 of ^{i}*Pr*).^{13}C NMR:(400 MHz, DMSO-d6) δ ppm: 170.81 (*C*=O); 152.98(*C*-O), 134.64(*C*-N), 121.20, 119.16 (*Ph*) ; 50.92 (N*C*H_2CO); 48.71 (*C*Hof ^{i}Pr); 23.11 (-CH_3). (DEPT-135, DMSO-d6) δ ppm: 121.21, 119.16 (*Ph*); 50.92 (N*C*H_2CO); 48.71 (*C*Hof ^{i}Pr); 23.11 (*C*H_3 of ^{i}Pr).

4,4'-bis(2-(n-butylamino)acetamido)diphenylether (L^3): MW: 426.56, Yield: 664.5 mg, 78%. m.p. 93 °C. ES-MS: 428.40 (M+2H). FTIR (KBr disc, cm^{-1}): 3284.24s, 2957.46s, 2930.99s, 2866.14m, 1677.67s, 1605.69m, 1541.36m, 1501.01s, 1409.80m, 1299.38m, 1228.24s, 1106.11m, 1013.34m, 943.15m, 880.34w, 836.64s, 737.53w, 704.03w, 604.85m, 511.66m, 433.61w. ^{1}HNMR:(DMSO-d6, 400 MHz) : δ (ppm) 9.36 (s, 4H, CON*H*) ; 7.56-6.97 (d, 8H, *Ph*); 3.38 (s, 4H, NCH_2CO); 2.68 (s, 4H, NCH_2 of ^{n}*Bu*); 1.70 (broad s, 2H, N*H*); 1.53-1.38 (m, 8H, CH_2 of ^{n}*Bu*); 0.97-0.93 (m, 6H, CH_3 of ^{n}*Bu*).^{13}C NMR:(400MHz, DMSO-d6) δ ppm: 170.65 (*C*=O); 152.95(*C*-O);134.71(*C*-N), 121.27 121.19, 119.13 (*Ph*); 53.28 (N*C*H_2CO); 49.29 (N*C*H_2 of ^{n}*Bu*); 32.11, 20.36 (*C*H_2 of ^{n}*Bu*) 14.38 (*C*H_3 of Butyl).(DEPT-135, DMSO-d6) δ ppm: 121.19, 119.14 (*C*H of Ph); 53.28 (N*C*H_2CO); 49.29 (N*C*H_2 of ^{n}*Bu*); 32.11, 20.36 (*C*H_2 of ^{n}*Bu*).

5.2.3. General Synthetic procedure for metallomacrocyclic dithiocarbamate complexes 1a-1c, 2a-2c, 3a- 3c

1 equivalent of diamine precursor L^1 (0.239 g, 0.5mmol), L^2 (0.199 g, 0.5mmol) or L^3 (0.213 g, 0.5mmol), was taken in acetonitrile and stirred vigorously. To this solution an

excess amount of NaOH (~3 equivalent; ~ 0.060 g) and carbon disulfide (~10 equivalent; ~ 0.5 ml) were added and stirred for 14 h at room temperature. A gradual change in colour was observed from colorless to a distinct yellow hue. $Ni^{II}(C_2H_3O_2)_2.4H_2O$ (136 mg, 0.55 mmol), $Cu(OAc)_2.H_2O$ (0.111 g, 0.55 mmol)or $Zn^{II}(C_2H_3O_2)_2.2H_2O$ (121 mg, 0.55mmol), dissolved in a minimum amount of distilled water was poured to this solution and stirred for further 9 hours. TLC was carried out to monitor the reaction progress. Rapid color change from pale yellow to dark green (in case of Ni^{II}), dark brown (in case of Cu^{II}) and to bright yellow (in case of Zn^{II}) was observed. The mixture was vacuum dried and washed with cold distilled water, followed by n-hexane and diethyl ether. The ensuing free flowing powder was vacuum dried under N_2 atmosphere to produce the corresponding macrocyclic dithiocarbamate complexes **1a-1c, 2a-2c, 3a-3c.**

[Ni$_2$-μ^2-bis-{(κ^2*S,S*-S$_2$CN(Cy)CH$_2$CONHC$_6$H$_4$)$_2$O}] (1a): Dark green MW: 1375.15, Yield: 285.3 mg, 83%. m.p. 234°C dec. FTIR (KBr disc, cm^{-1}): 3313.82w, 3296.46w, 3284.88w, 2933.83s, 2855.67s, 1693.56s, 1668.48m, 1608.69w, 1508.38s, 1475.59m, 1456.30m, 1417.73m, 1373.36w, 1329.00m, 1305.86w, 1248.08s, 1192.05w, 1170.83m, 1139.97w, 1106.25m, 1012.66s, 974.08s, 916.22w, 875.71m, 852.56m, 831.35w, 526.58m.^{1}H NMR (DMSO-d_6, 400 MHz): δ (ppm) 10.18 (s, 4H, CON*H*); 7.67-6.93(m, 16H, *Ph*); 4.45 (s, 8H, NC*H*$_2$CO); 4.33 (s, 4H, C*H* of Cy); 1.90-1.10 (m, 20H, *Cy*).^{13}CNMR (400 MHz, DMSO-d_6): δ ppm: 207.21 **(-N^{13}*C*S$_2$)**, 164.45 (*C*=O), 153.11 (*C*-O), 135.48, 134.62 (*C*-N), 127.55, 121.18, 119.26, 118.33, 117.60 (*Ph*), 59.43 (N*C*H$_2$CO), 48.30 (*C*H of *Cy*), 29.62, 29.37, 25.40, 24.90 (*C*H$_2$ of Cy).

[Cu$_2$-μ^2-bis-{(κ^2*S,S*-S$_2$CN(Cy)CH$_2$CONHC$_6$H$_4$)$_2$O}] (1b). Brown; MW: 1384.86, Yield: 249.1 mg, 72 %; m.p. 216 °C dec. ES-MS: 1423.3 (M+K). FTIR (KBr disc, cm^{-1}): 3502.85w, 3256.95m, 3219.30m, 2995.55w, 2933.83s, 28, 2856.67m, 1699s, 1543.10s, 1525.74s, 1498.74s, 1452.45m, 1224.84s, 1163.11w, 1109.11s, 1076.32s, 621.10s, 472.58m, 418.57s.

[Zn$_2$-μ^2-bis-{(κ^2*S,S*-S$_2$CN(Cy)CH$_2$CONHC$_6$H$_4$)$_2$O}] (1c). Yellow; MW: 1388.53, Yield: 235.9 mg, 68%; m.p. 226 °C dec. FTIR (KBr disc, cm^{-1}): 3309.96w, 3291.53w, 3286.81s, 2931.90s, 2854.74s, 1666.55s, 1643.41m, 1608.69m, 1536.39s, 1500.67vs,

1152.45s, 1408.08s, 1375.29w, 1288.70vs,1228.70s,1166.97m,1139.97w,1105.25w,1010.73s,972.16m,877.61m,852.56m , 831.35w,665.46m, 515.01m, 484.15m,472.58m. ^{1}H NMR (DMSO-d$_6$, 400 MHz) δ, ppm: 10.02 (s, 4H, CON*H*); 7.65-6.91 (d, 16H, *Ph*); 4.82 (s, 8H, NC*H*$_2$CO); 4.54 (m, 4H, C*H* of Cy); 1.89-1.11(m, 20H, *Cy*). ^{13}C NMR (400 MHz, DMSO-d$_6$) : δ 206.15 **(-N^{13}*C*S$_2$)**, 165.73 (*C*=O), 152.92 (*C*-O) 135.03, 130.86 (*C*-N), 121.04, 120.87, 119.18, 117.51 (*Ph*), 64.16 (N*C*H$_2$CO); 51.93, 49.38 (*C*H of *Cy*); 30.05-21.53 (*C*H$_2$ of Cy).

[Ni$_2$-μ^2-bis-{(κ^2*S,S*-S$_2$CN(*^{i}Pr*)CH$_2$CONHC$_6$H$_4$)$_2$O}] (2a). dark Green; MW: 1214.,89, Yield: 236.7 mg, 78%; m.p. 223 °C dec.ES-MS: 1215.4 (M+H). FTIR (KBr disc, cm^{-1}): 1666.55s, 1498.74s, 1485.95s, 1410.01m, 1305.85m, 1228.70s, 1170.83m, 1072.46m, 833.28m. ^{1}H NMR (400 MHz, DMSO-d$_6$): δ (ppm) 10.13 (s, 4H, CON*H*); 7.44-6.88 (m,16H,*Ph*) ; 4.51 (s, 8H, NC*H*$_2$CO); 4.25 (s, 4H, C*H* of ^{i}Pr); 1.08 (d, 24H, C*H*$_3$).^{13}CNMR(400 MHz, DMSO-d$_6$) δ ppm: 206.86 **(-N^{13}*C*S$_2$)**, 164.43 (*C*=O), 127.54, (*C*-N); 121.16, 120.31,119.23, 118.30 (*Ph*), 53.36, 51.44 (N*C*H$_2$CO); 47.45 (*C*H of ^{i}Pr), 19.37 (*C*H$_3$of ^{i}Pr).

[Cu$_2$-μ^2-bis-{(κ^2*S,S*-S$_2$CN(*^{i}Pr*)CH$_2$CONHC$_6$H$_4$)$_2$O}] (2b). Dark Brown; MW: 1224.60, Yield: 198.9 mg, 65%; m.p. 172 °C dec. FTIR (KBr disc, cm^{-1}): 3271.38m, 2978.19m, 1672.31s, 1546.96m, 1537.32m, 1500.7vs, 1464.02s, 1408.08m, 1303.92m, 1230.63s, 1182.40w, 1130.32w, 1107.18w, 1074.39w, 829.42m.

[Zn$_2$-μ^2-bis-{(κ^2*S,S*-S$_2$CN(*^{i}Pr*)CH$_2$CONHC$_6$H$_4$)$_2$O}] (2c). Pale Yellow; MW: 1228.27, Yield: 178.0 mg, 58%; m.p. 182 °C dec. ES-MS: 1226.7 (M-2H). FTIR (KBr disc, cm^{-1}): 3284.88m, 2931.90s,2854.74s,1672.34s, 1606.76w, 1535.39m, 1498.74vs, 1452.45m, 1408.08m, 1193.98w, 1010.73s, 833.28s, 511.15m.^{1}H NMR(DMSO-d6, 400 MHz): δ (ppm) 10.05 (s, 4H, CON*H*); 7.55-6.91 (m, 16H, *Ph*); 5.21 (s, 8H, NC*H*$_2$CO); 4.48 (s, 4H, C*H* of *^{i}Pr*); 1.18-1.16 (m, 24H, C*H*$_3$ of ^{i}Pr).^{13}C NMR (400 MHz, DMSO-d$_6$) δ ppm: 206.24 **(-N^{13}*C*S$_2$)**; 165.78(*C*=O), 152.91(*C*-O), 135.04, 130.85(*C*-N), 121.02, 120.87, 120.76, 119.17 (*Ph*); 64.08, (N*C*H$_2$CO); 51.94 (*C*H of ^{i}Pr); 30.06-25.18 (*C*H$_3$ of ^{i}Pr).

[Ni$_2$-μ^2-bis-{(κ^2*S,S*-S$_2$CN(*^{n}Bu*)CH$_2$CONHC$_6$H$_4$)$_2$O}] (3a). Dark Green; MW: 1271.00, Yield: 273.2 mg, 86 %; m.p. 252 °C dec. FTIR (KBr disc, cm^{-1}): 3298.38s, 2958.90s, 2929.97s, 2870.17m, 1678.13s, 1608.69m, 1498.74vs, 1303.92m, 1222.91s, 1111.03m, 1012.66m, 833.28m, 513.08m.^{1}H NMR(DMSO-d6, 400 MHz): δ (ppm) 10.24 (s, 4H, CON*H*); 7.53-6.93 (d, 16H, *Ph*); 4.41 (s, 8H, NC*H*$_2$CO); 3.40 (s, 8H, NC*H*$_2$ of *^{n}Bu* merged with DMSO-d$_6$); 1.56, 1.25 (m, 16H, C*H*$_2$ of *^{n}Bu*) 0.86 (m, 12H, C*H*$_3$ of *^{n}Bu*).^{13}C NMR(400 MHz, DMSO-d$_6$) δ ppm: 207.21 **(-N^{13}*C*S$_2$)**, 164.20 (*C*=O), 153.14 (*C*-O), 134.51(*C*-N), 121.21, 119.28 (*Ph*), 51.90 (N*C*H$_2$CO); 51.19 (N*C*H$_2$ of *^{n}Bu*); 28.71, 19.81 (*C*H$_2$ of *^{n}Bu*); 14.06 (*C*H$_3$ of ^{n}Bu).

[Cu$_2$-μ^2-bis-{(κ^2*S,S*-S$_2$CN(*^{n}Bu*)CH$_2$CONHC$_6$H$_4$)$_2$O}] (3b). Brown; MW: 1280.71, Yield: 230.4 mg, 72%; m.p. 226 °C dec. ES-MS: 1281.6 (M+H). FTIR (KBr disc, cm^{-1}): 3275.24m, 1674.27s, 1608.69w, 1546.96m, 1537.32m, 1498.74s, 1302.92m, 1222.91s, 1168.90w, 1141.90w, 1111.03m.

[Zn$_2$-μ^2-bis-{(κ^2*S,S*-S$_2$CN(*^{n}Bu*)CH$_2$CONHC$_6$H$_4$)$_2$O}] (3c). Yellow; MW: 1284.37, Yield: 276.0 mg, 86%; m.p. 234 °C dec. ES-MS: 1323.8 (M+K). FTIR (KBr disc, cm^{-1}): 3275.24m, 2966.97s, 2929.97s, 2872.10w, 1670.41s, 1535.39m, 1498.74s, 1301.99w, 1222.91s, 1126.47w, 1109.11w, 1006.88m, 970.23m, 831.35s, 513.08m, 493.79m.^{1}H NMR (DMSO-d6, 400 MHz): δ (ppm) 10.09 (s, 4H, CON*H*); 7.64-6.55 (m, 16H, *Ph*); 4.65 (s, 8H, NC*H*$_2$CO); 3.85 (s, 8H, NC*H*$_2$ of *^{n}Bu*); 1.83-1.23 (m, 16H, C*H*$_2$ of ^{n}Bu); 0.91-0.84 (m, 12H, C*H*$_3$ of ^{n}Bu). ^{13}C NMR (400 MHz, DMSO-d$_6$) δppm: 206.92 **(-N^{13}CS$_2$)**, 165.70 (C=O), 152.96 (*C*-O), 134.93(*C*-N), 121.33, 121.08, 120.81, 119.20 (*Ph*), 57.39 (N*C*H$_2$CO), 56.58 (N*C*H$_2$ of *^{n}Bu*), 28.82, 19.99 (*C*H$_2$ of *^{n}Bu*); 14.20 (*C*H$_3$ of *^{n}Bu*).

5.2.4. *In vitro* cytotoxicity studies

5.2.4.1. Cell line and Culture

The cell lines (HepG2 and WRL-68) were procured from the National Centre for Cell Science, Pune; pre-cultured in DMEM supplemented medium (containing 10% fetal

bovine serum and 1% antibiotics) in tissue culture flasks. Cultured cells were incubated at 37°C in humidified atmosphere containing 5% CO2. DMEM medium was changed every third day and cell growth was monitored microscopically. Cells were regularly trypsinized (0.1% trypsin EDTA 0.02%, dextrose 0.05%).

5.2.4.2. MTT assay for cell viability/ proliferation

For testing cytotoxicity potential of test compounds- **L**, **L'**, $\mathbf{L^1}$, $\mathbf{L^2}$, $\mathbf{L^3}$ and their ensuing complexes, MTT assay was performed. In a 96 well plate, HepG2 cells were plated (10^3cells / well in 100 µL of medium) in their exponential growth phase, for 24 hr. Test compounds were prepared in 5% DMSO and cells were exposed to different concentration of test compounds (6.25µg/ml, 12.5µg/ml, 25µg/ml, 50µg/ml and 100 µg/ml) for 24 hrs. Post incubation media was removed and cells were incubated with 10µL of MTT reagent (5mg/ml) at 37^0C for 4hrs. DMSO was used to solubilize formazan crystals, produced by only viable cells. The optical density was measured at 540nm by an ELISA reader (BIOTEK ELX800 Universal Microplate Reader).[3] Percentage cytotoxicity was calculated against control (media with DMSO only) for all the test compounds.

5.2.4.3. Statistical analysis for determination of IC_{50}

Data obtained was analyzed in Prism/OriginPro 8 for standard error and probit analysis. The percent cytotoxicity index (% CI) was calculated as follows:

% CI= [1− (OD of treated cells/ OD of control cells)] × 100 %

where, CI= cytotoxicity index, OD= optical density.

A plot of % CI versus concentration was obtained from the experimental data for each set of experiments. The values of IC_{50} (50% growth inhibition of cell) were determined from the graph.

5.2.4.4. Assessment of apoptosis AO/EtBr staining

Cells were grown in 24 well-plate (5 x 10^5) and were incubated in a CO_2 incubator at 37^0C. Cells were dosed with IC50 concentration of compounds. After 24hrs of incubation, cells were washed with PBS and stained with 200µl of AO-EtBr mixture (100µg/ml AO: 100µg/ml EtBr). Cells were observed under FLoid™ Cell Imaging Station (Life Technologies) fluorescent microscope at 20X magnification.[39]

5.3. Result and Discussion

5.3.1. Syntheses and characterization

Towards our search for better cytotoxic agents,[14, 18-19] a new series of binuclear dithiocarbamate macrocyclic complexes **1a-1c, 2a-2c, 3a-3c** bearing functionalized polar linker and biologically active transition metal fragment have been designed and synthesized via a room temperature single-pot reaction protocol involving self-assembly of the corresponding diamines viz. 4,4'-bis(2-(cyclohexylamino)acetamido)biphenylether (L^1), 4,4'-bis(2-(isopropylamino)acetamido)diphenyl ether (L^2) or 4,4'-bis(2-(n-butylamino)acetamido)diphenyl ether (L^3) The overall reaction presented in Scheme 1 and 2. with CS_2 and transition metal ion viz. Ni^{II}, Cu^{II} or Zn^{II} in moderate to good yields as illustrated in Scheme 3. The diamine precursors (L^1-L^3) were prepared according to the literature procedure. It is predicted that the presence of several alkyl groups, biologically active amide functionalities and dithiocarbamate subunits present as well as ether (–O–) linkage in the molecular framework of **1a-1c, 2a-2c, 3a-3c** would conjointly expedite the interaction with biomolecules through potential donor-acceptor relations such as hydrogen bonding, CH-π, π-π interactions.

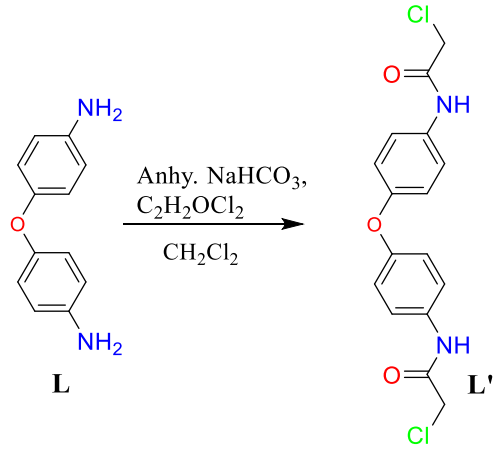

Scheme 1: Reaction scheme for 4,4'-bis(2-chloroacetamido)diphenyl ether (**L'**)

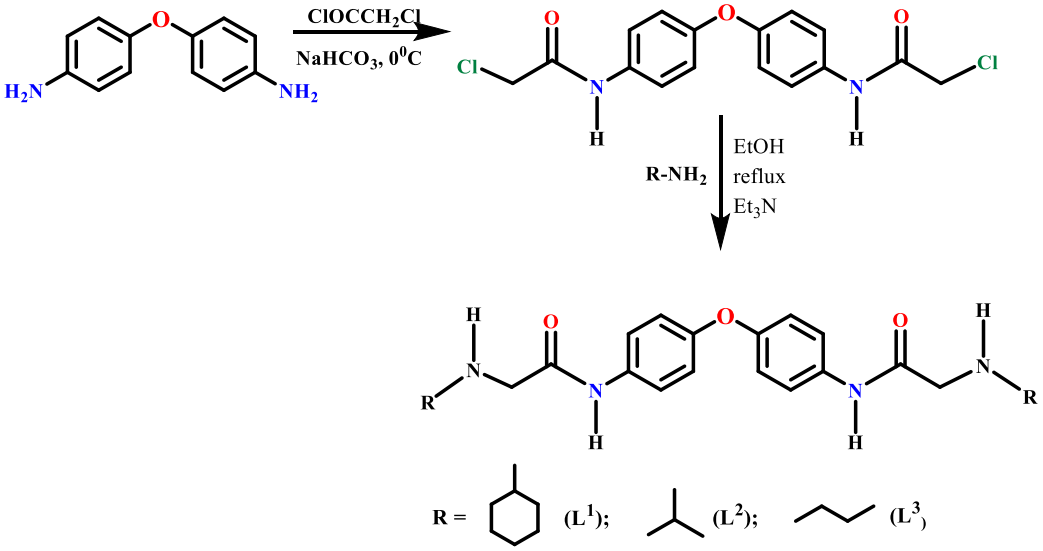

Scheme 2: Preparation of 2° diamine precursors $\mathbf{L^1}$-$\mathbf{L^3}$.

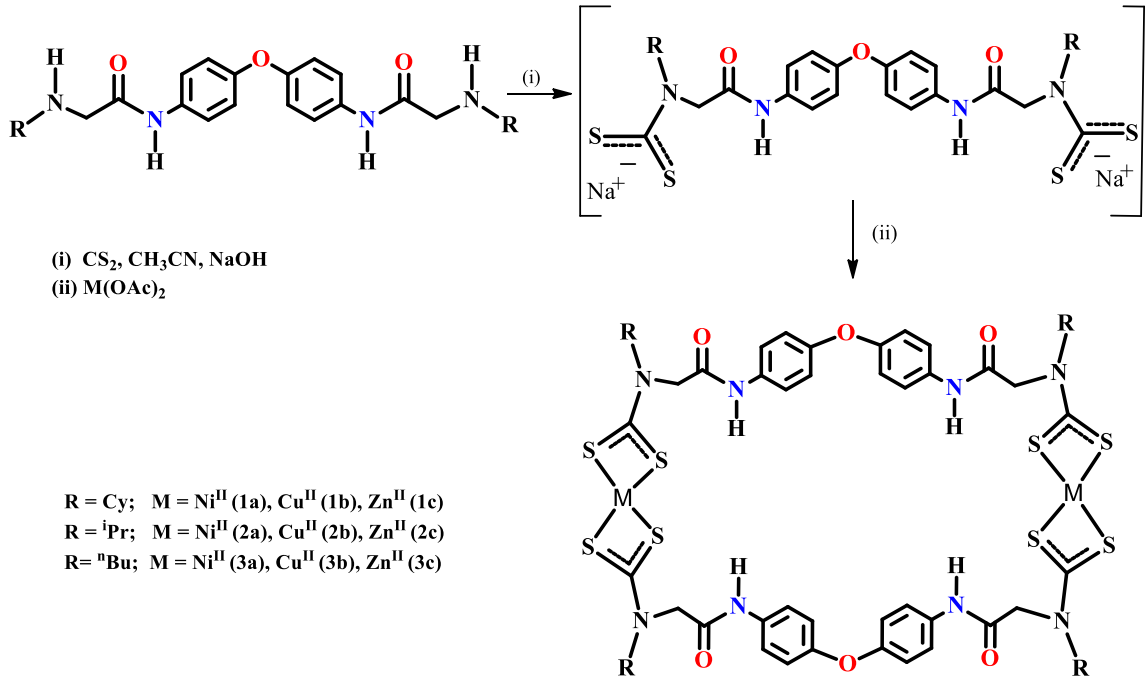

Scheme 3: Single-pot Synthetic methodology adopted for metallomacrocyclic dithiocarbamate macrocyclic complexes **1a-1c**, **2a-2c** and **3a-3c**.

5.3.2. NMR, Mass and IR spectral study

The distinctive ^{1}H NMR signals for amide protons (CON*H*) and α-methylene protons (NC*H*$_2$CO) in **L^1-L^3** appeared at ~9.91 ppm and at ~3.44 ppm. The characteristic amine –NH signal appeared as a broad peak in the range of 2.02-1.70 ppm. Multiplets corresponding to methylene/ methine protons as well as other signals corresponding to the protons of aromatic and N-alkyl substituents appeared in the expected range. The characteristic ^{13}C NMR signals corresponding to carbonyl, the α-methylene (N*C*H$_2$CO) and aliphatic *N*-substituents (N*C*H/ N*C*H$_2$) appeared exclusively in the range of 170.38-170.81 ppm, 50.92-61.91 ppm and 48.71-56.72 ppm. DEPT-135 experiment well supported the assignments of ^{13}C NMR signals for **L^1-L^3**. (Annexure 18-26) The ES-MS spectra of **L^1 and L^3** gave molecular ion peaks at 478.59 and 428.40 which correspond to

[M^+] and [M+2H] along with the anticipated fragments. (Annexure 1) The representative IR bands for $\mathbf{L^1}$-$\mathbf{L^3}$ appeared in the range of 3559-3131 cm^{-1}, 3050-2851 cm^{-1}, 1677-1672 cm^{-1}, 1604-1526 cm^{-1} and 1409-925 cm^{-1}, attributed to ν(N-H), aromatic ν(C-H), ν(C=O), ν(C=C) and ν(C-N) stretching vibrations respectively. (Annexure 10, Annexure 14) These experimental data are consistent with the literature reports.[14] The bimetallic macrocyclic dithiocarbamate complexes (**1a-1c, 2a-2c** and **3a-3c**) were satisfactorily characterized by various spectroscopic techniques viz. ESI-MS, FTIR, NMR (^{1}H, ^{13}C, DOSY), UV-visible. DFT level calculations were further carried out on representative compounds in order to validate the experimental outcomes. The composition and phase purity of the complexes have been confirmed by characteristic ^{1}H and ^{13}C and by ^{1}H-DOSY NMR signals. The peaks corresponding to the ligand functionalities in the ^{1}H NMR spectra of the complexes appear very well in the expected range. Distinctly, in the ^{13}C NMR spectra, all the diamagnetic complexes showed a single distinct downfield resonance at δ 206–207 ppm associated with the N–CS_2unit.[18, 26-28] (Annexure 28, 30, 32 and Annexure 34). Compared to those of the free diamine precursors substantial shifting of ^{1}H/^{13}C signals associated with *N*-methylene and *N*-methine reinforce the formation of proposed structures. Significant factors like stereo-electronic features of ligand framework, thermodynamic conditions and metal centres primarily decides the progress of coordination driven self-assembly of a discrete molecular structures.[29-30] The presence of anticipated signals and absence of signals corresponding to uncoordinated end groups in the NMR spectra of **1a, 1c, 2a, 2c, 3a** and **3c** ruled out the possibility of formation of oligomers or coordination polymeric products. (Annexure 27-34) The ^{1}H DOSY NMR spectral analysis of complexes **1a** (Fig. 1) and **3c** (Fig. 2), explicitly display the presence of only one type of species in solution and rule out the possibility of formation of oligomers or coordination polymers. The ESI-MS spectra of these complexes gave m/z molecular ions peaks at 1423.3, 1215.4, 1226.7, 1281.6, 1323.8 for **1b**, **2a**, **2c**, **3b**, **3c** respectively which corresponds to either [M+H], [M+K] or [M-2H] molecular ions. (Annexure 2, 3, 4, 5, 7, 8, and Annexure 9) The IR spectra of these complexes show the ν(C–N) and ν(C–S) frequencies at 1498–1408 and 1076–1006 cm^{-1} respectively characteristic of the dithiocarbamate ligand coordination. Besides, a medium to weak

intensity ν(M-S) bands are observed in the 526-418 cm^{-1} range which is in agreement with the earlier observations.[31] (Annexure 11, 12, 13, 15, 16 and Annexure 17)

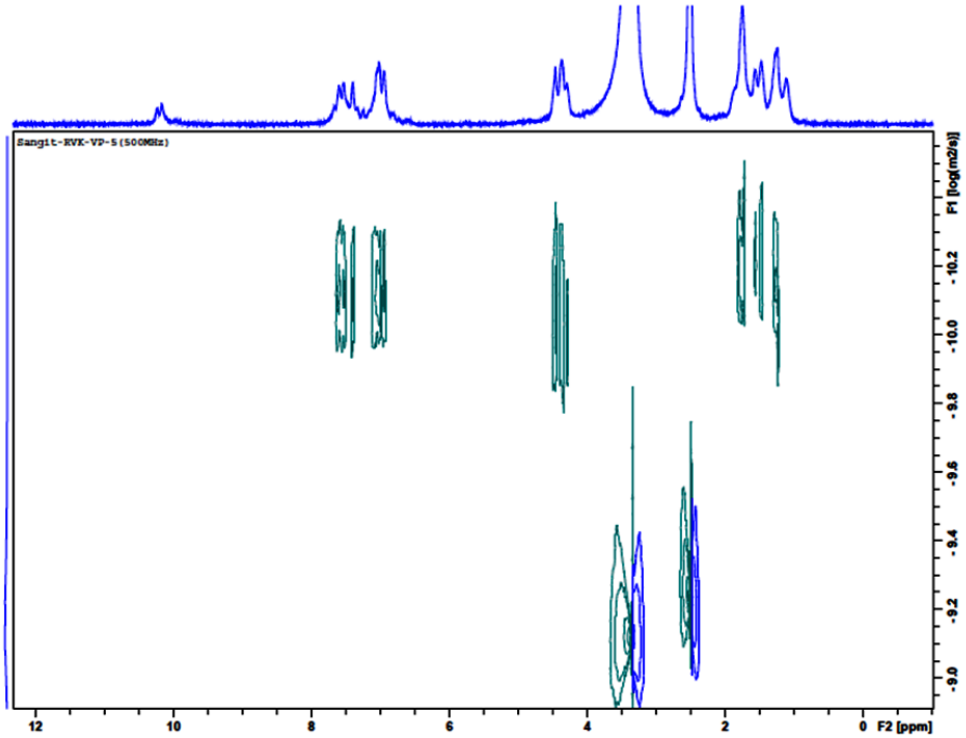

Fig. 1. ^{1}H DOSY NMR spectrum of **1a**.

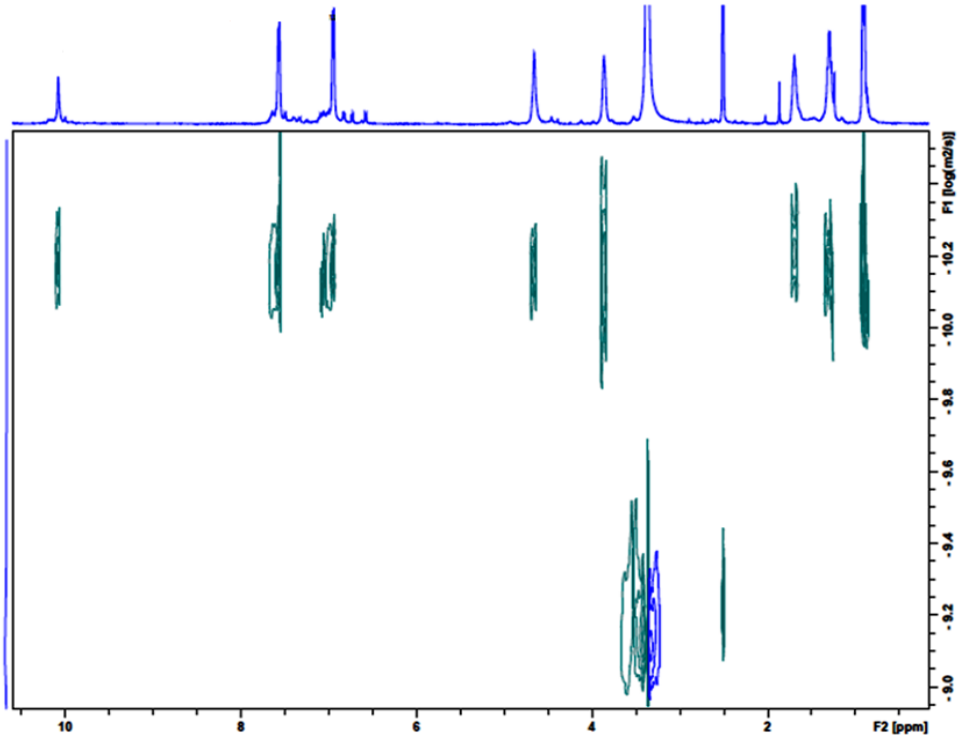

Fig. 2. ^{1}H DOSY spectrum of **3c.**

5.3.3. UV-visible absorption, magnetic moment and fluorescence emission study

The UV-visible absorption spectra of **L^1-L^3** display a single evident band at shorter wavelength at ~300 nm assignable to π→π* (phenyl) transitions. However, binuclear complexes 1a, 2a and 3a show three notable bands in the region of 321-326, 381-392 and 468-479 nm corresponding to intra-ligand π→π*, n→π* and L→M charge-transfer transitions, respectively (Fig. 3 and Table 1). The presence of amide groups causes these lower energy charge-transfer transitions owing to their electron withdrawing nature.[32] Apart from the bands due to π→π* and L→M charge-transfer transitions a prominent band appears at ~ 630-639 nm which is attributed to d-d transition [33] in case of copper complexes **1b**, **2b**, **3b**. All the newly synthesized compounds were also studied for their fluorescence properties (Annexure 35). Compounds **1a-1c** effectively quenched the ligand L^1 flouroscence upon excitation at 326 nm which is similar to the earlier observation by us previously.[19] The presence of the unpaired *d* electron in the complexes of fluorescent ligands with transition metals makes them an effective fluorescence quenchers.[18,34]

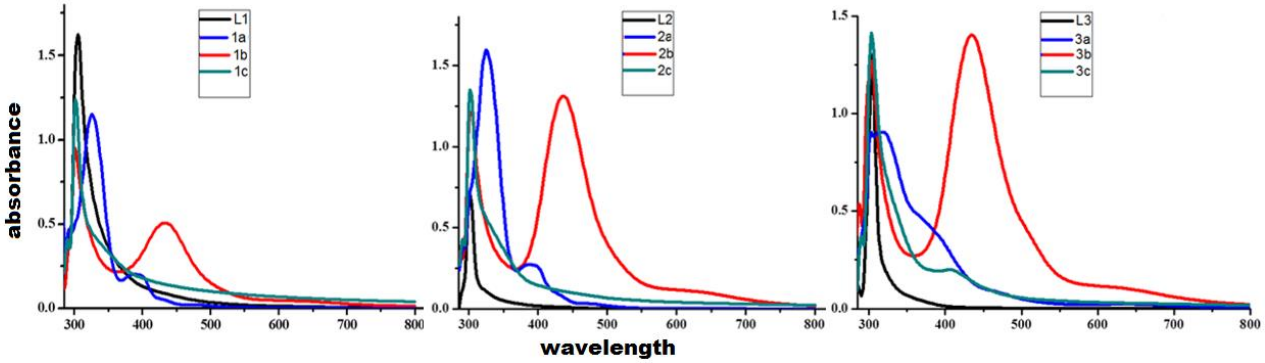

Fig. 3. Absorption spectra of **L^1-L^3** and their metallomacrocyclic dithiocarbamate complexes **1a-1c**, **2a-2c** and **3a-3c** in DMF solution.

Table- 1
UV-visible absorption, magnetic moment and fluorescence data for the compounds

Entry	UV-visible spectral data (10^{-3} M DMF) λ_{max} nm (ε, $LMol^{-1}cm^{-1}$)	Wave number	Magnetic Moment μ_{eff}(BM)	Fluorescence spectral data (10^{-3} M DMF)	
				λ_{ex} nm	λ_{em}(nm) (Intensity)
L^1	305 (1627) π→π*	3278	-	305	478 (17) π*→π

L^2	301 (722.2) π→π*	3322	-	301	327 (17)
L^3	303(1302.6) π→π*	3300	-	303	328 (2) π*→π
1a	326 (34549) π→π*; 392 (6072) n→π*; 479(681.68) charge transfer	3067, 2551 2087	dia	326	361(4)
1b	301 (3572) π→π*; 433 (1907) charge transfer 639(167.29) *d-d transition*	3322 2309 1564	1.89	---	Non Fluorescent
1c	302 (9296) π→π*; 354 (2350) n→π*	3311,2824	dia	302	356(4) π*→π
2a	325 (47896) π→π*; 391 (8148) n→π* 478(945.09) charge transfer	3076, 2557 2092	dia	325	388(15) π*→π
2b	303 (9097) π→π* 436 (9855) charge transfer 631 (816.20) *d-d transition*	3300 2293 1584	1.90	---	Non fluorescent
2c	302 (8092) π→π*; 335 (2849) n→π*	3311,2985	dia	302	365(15) π*→π
3a	321 (27095) π→π*; 381 (12484) n→π*, 469 (2541) charge transfer	3115, 2624 2132	dia	321	425(3)
3b	303 (7604) π→π* 435 (8434) charge transfer 630 (635) *d-d transition*	3300 2298 1587	1.87	303	361(5)
3c	302 (8489) π→π*; 408 (1204) n→π*;	3311, 2450	dia	302	362 (17) π*→ π

Nevertheless, in several occasions numerous diamagnetic Ni(II) complexes with square planar geometry have appeared as effective fluorescence quenchers with quenching rates as high as 10^{10} dm^3 mol^{-1} s^{-1}.[35] Ligand precursor **L^3** appeared to be non-fluorescence, however its complex derivatives 3a-3c fluoresces significantly with concomitant Stoke shifting of ~ 32 nm. The overall fluorescence property of these transition metal dithiocarbamate complexes is consistent with our earlier observations.[19, 26, 28] Magnetic moment values, NMR studies and UV-visible absorption bands undoubtedly suggest square planar/distorted square planar environment around Ni^{II}/ Cu^{II} centers and tetrahedral/distorted tetrahedral environment around Zn^{II} centers in their corresponding complexes[19,36] which is further reinforced by DFT calculation performed at B3LYP/LanL2DZ level discussed latter.

5.3.4. Thermogravimetric study

Under N_2 atmosphere thermogravimetric plots of L^1-L^3 and their metal complexes 1a-1c, 2a-2c and 3a-3c, (Annexure 36-42) were recorded rom room temperature to 550 °C at a heating rate of 10 °C/min. TG curves revealed the single/ multistage thermal degradation of the diamine precursors as well as binuclear complexes whereas at different temperatures DTG curves displayed maximum rate of degradation for these compounds. Except **L^1** all other compounds showed distinct multistage thermal degradation patterns on their respective TG curves. All the complexes appear to be thermally stable at about 100-120° C. The thermal decompositions of all the complexes start before their melting points and accompanied by the appearance of one or more endothermic peak on corresponding DTA curves. The intermolecular interactions in the solid state decides the thermal stability as well as assortment in the thermal degradation pattern of these compounds. The thermal decomposition patterns of these complexes are consistent with the patterns observed for analogues compounds.[19]

5.3.5. Geometry Optimization

DFT level calculations and full geometry optimization of some representative compounds viz. diamine precursor **L^1** as well as complexes **1a-1c** (Fig. 4) has been executed using B3LYP/6-31G (d, p) and B3LYP/LanL2DZ basis sets. Gaussian 03 program suite[37] has been used for calculations and molecular orbitals were generated by GaussView 3.0 program. Recent Literature demonstrates the use of analogues calculations to achieve appreciable results for bulky molecular structures.[38] The substantial deviations in the electronic structural parameters like in case of Ar-O-Ar angles amongst **L^1** and its dithiocarbamate complexes **1a-1c** decreases significantly from 119.6 Å to 117.1 Å and also increases to as high as 122.80 in one of the linker fragments of **1c** which confirms the flexibility associated with the –$(CH_2CONHC_6H_5)_2O$– linker framework which along with loss of coplanarity of the amide group could be an crucial factor for effective contacts with biomolecules. The structural parameters such as bond lengths and bond angles deduced for **1a-1c** theoretically were found to be consistent with the similar

parameters obtained experimentally by X-ray study of closely related compounds. (Table 2)[39] The DFT study clearly reveals that both the phenyl groups of $\mathbf{L^1}$ forms a dihedral angle of 82.42º that confirms the existence of diversified *'gauche'* conformation whereas the similar angle in its transition metal dithiocarbamate complexes **1a-1c** appeared in the range of 56.57º -69.80º. This decrease in the dihedral angle facilitates the formation of the macrocyclic arrangement in the molecular structure after coordination the transition metals in **1a-1c**. The geometries of **1a-1c** clearly reveal bimetallic macrocyclic distorted square planar geometry around nickel(II)/ copper (II) centers and distorted tetrahedral geometry around zinc(II) center in **1a-1c** with the two ligand molecules bridged over two metal centres *via* chelating sites of terminal dithiocarbamate moieties. Out of the four *N*-Cy one of the cyclohexyl ring substituent in the macrocyclic architecture of **1a, 1b** is exposed towards the inner side of the 44-member molecular cavity which can be visualized in the optimized geometry (Fig. 4) and in the spacefilled model (Fig. 5) of **1a, 1b**. M-S bond distances of 2.43-2.45 Å and 2.39-2.41 Å in zinc (II) complex **1c** explains its anisobidentate mode of the -NCS_2 moieties and an isobidentate coordination mode in nickel(II) **1a** and copper(II) **1b** complexes is reflected by **1a** and **1b** M-S bond distances of 2.16-2.22 Å and 2.37-2.40 Å. These observations are fairly comparable with the experimental data as well as with the theoretical data calculated by us recently.[40] The transannular M···M distances of these 44-membered macrocycles **1a-1c** were observed to be 13.213, 13.281 and 14.314 Å which are quite similar to the analogous structures.[40]

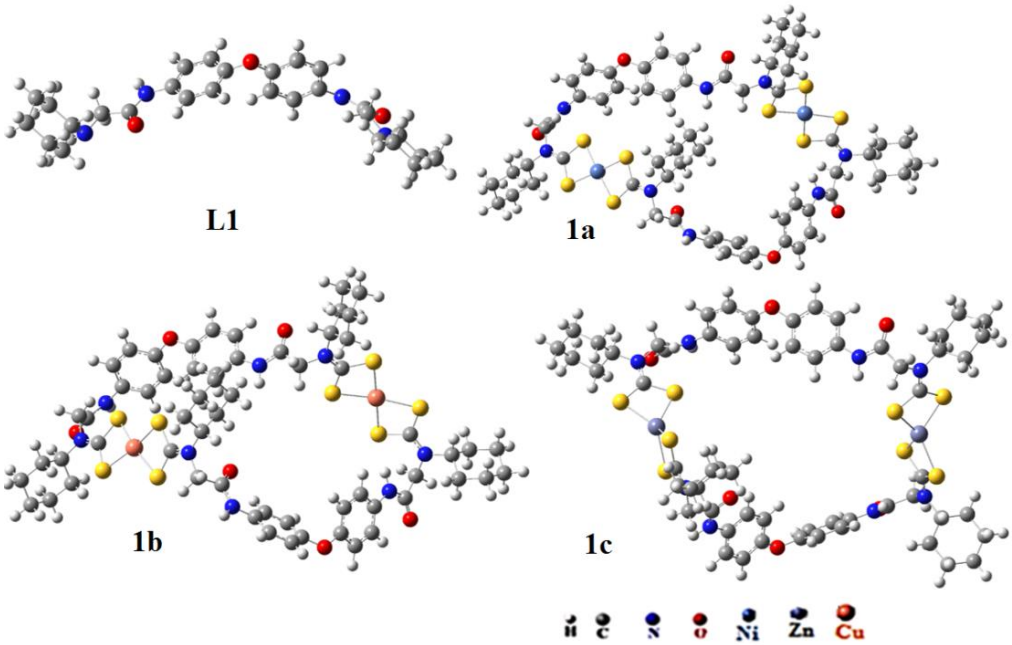

Fig. 4. An optimized geometry for the minimum energy conformation for $\mathbf{L^1}$ and its dithiocarbamate complexes **1a-1c** at (B3LYP/6-31G (d, p) and B3LYP/LanL2DZ levels, respectively.

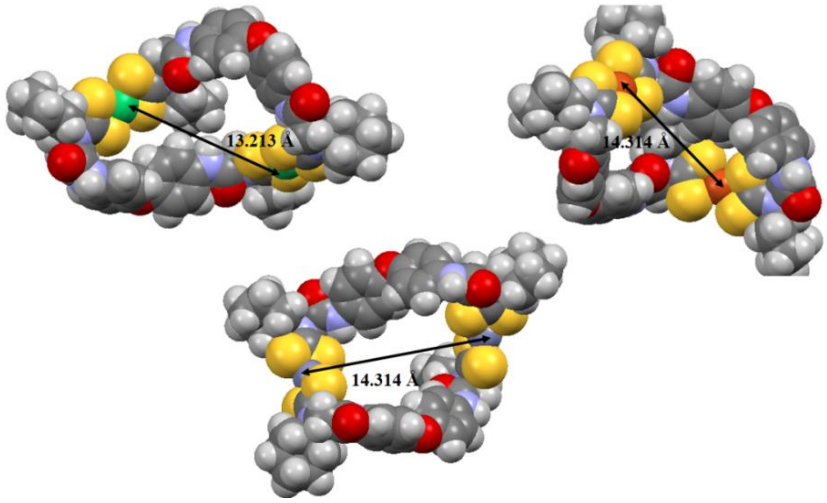

Fig. 5. Spacefilled representation of the optimized geometry revealing a cavity generated by the macrocyclic architecture of metallomacrocyclic dithiocarbamate complexes **1a-1c**.

It may be noted that the cavity produced by the macrocyclic framework of metallomacrocyclic dithiocarbamate complexes **1a-1c** is altered greatly by the presence of different transition metals (Fig. 5).

Table 2

Comparison of selected geometrical parameters for 1a-1c obtained from theoretical with similar experimental parameters retrieved from the literature.

Selected Bond	Bond lengths (Å)	Selected Bonds	Bond angles (°)
	1a		
N—C	1.340-1.345	S—Ni—S (chelate)	77.86-78.15
C—S	1.730-1.744	S—Ni—S	101.35-102.94
Ni—S	2.263-2.282		
Transannular Ni-Ni	13.213		
	Ni(II) dithiocarbamate based macrocycle [39a]		
N—C	1.281-1.508	S—Ni—S (chelate)	78.99-79.87
C—S	1.691-1.744	S—Ni—S	100.31-177.14
Ni—S	2.164-2.225		
	1b		
N—C	1.342-1.347	S—Cu—S (chelate)	75.06-75.14
C—S	1.734-1.746	S—Cu—S	104.30-107.67
Cu—S	2.378-2.409		
Transannular Cu-Cu	13.281		
	Cu(II) dithiocarbamate based macrocycle[39b]		
N—C	1.318-1.328	S—Cu—S (chelate)	77.59
C—S	1.719-1.727	S—Cu—S	101.72-103.48
Cu—S	2.288-2.301		
	1c		
N—C	1.342-1.353	S—Zn—S (chelate)	75.43-75.70
C—S	1.743-1.760	S—Zn—S	124.15-131.58
Zn—S	2.431-2.453		
Transannular Zn-Zn	14.314		
	Zn(II) dithiocarbamate based macrocycle[39c]		
N—C	1.333-1.363	S—Zn—S (chelate)	79.5-81.2
C—S	1.717-1.782	S—Zn—S	126.53-136.00
Zn—S	2.32-2.44		

Frontier molecular orbital analysis

The LUMO in **1a** (Fig. 6) is delocalized over both the phenyl rings adjacent to the ethereal oxygen of the one of the linker moiety and also on over the peripheral amide moiety. A slight delocalization of LUMO is also found over both the coordinated Ni^{II} metal centre. The HOMO of **1a** is exclusively delocalized on the π-system of phenyl rings. In **1b** and **1c,** LUMO is predominantly localized at one of the coordinated dithiocarbamate moiety whereas, the HOMO is situated over π-system of phenyl rings

and the peripheral amide groups. The calculated HOMO-LUMO energy gaps (Isovalue = 0.02) for **L**[1] and its corresponding metallomacrocyclic dithiocarbamate complexes **1a-1c** are given in Table 3 is illustrated in Fig. 6. The λ_{max} values obtained by computational study are similar with the λ_{max} values (Table 3) determined experimentally by means of UV-visible absorptions which further confirms the correlation of computational investigations with the experimental results.

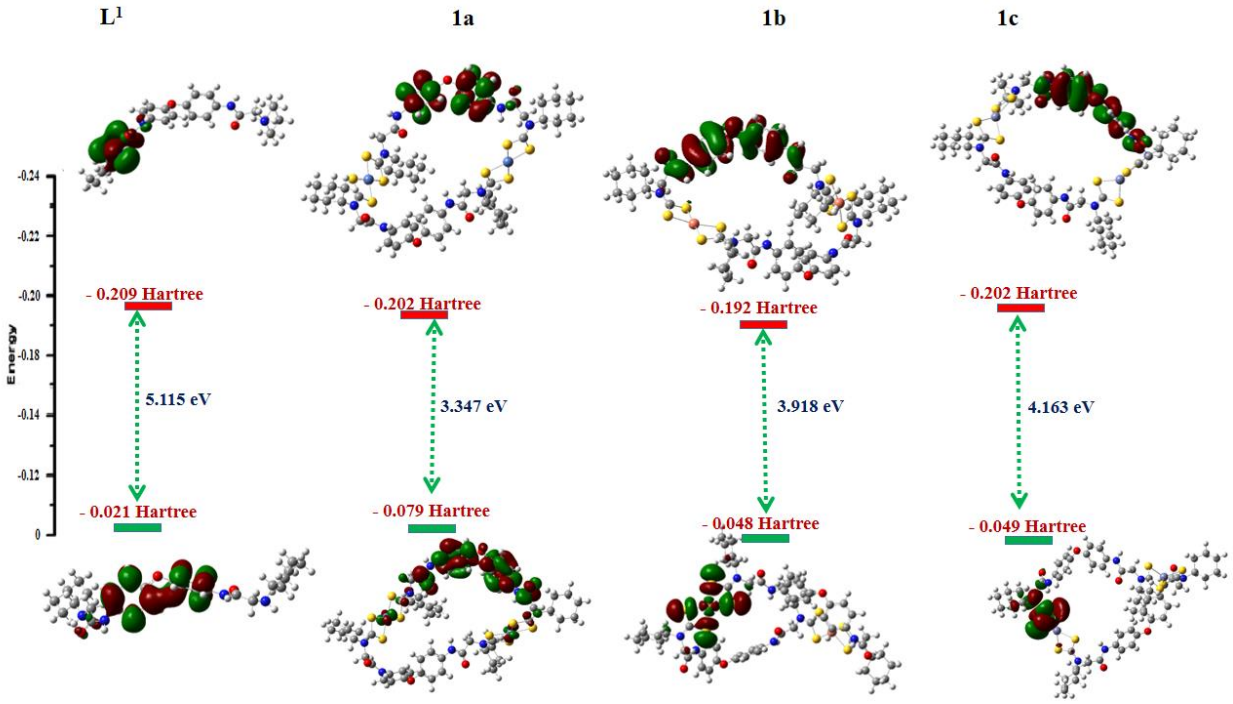

Fig. 6. Frontier molecular orbitals (Isovalue= 0.02) derived from DFT calculation at B3LYP/6-31G (d, p) level: for **L**[1]and at B3LYP/LAN2DZ level: for **1a-1c.**

Table 3

Summary of computational studies performed on **L^1** and **1a-1c**

Entry	Energy of optimized geometry (Hartree)	M…M Distance (Å)	E_{HOMO}, E_{LUMO} (Hartrees)	$\Delta E_{HOMO-LUMO}$ (eV)	λ_{max} calc. (expt.) nm
L^1	-1534.632	-	- 0.209, -0.021	5.115	242 (305)
1a	-6743.462	13.213	-0.202, -0.079	3.347	370 (392)
1b	-6797.118	13.281	-0.192, -0.048	3.918	316 (301)
1c	-6536.034	14.314	-0.202, -0.049	4.163	298(302)

Molecular electrostatic potential

The molecular electrostatic potential (MESP) of chemical species plays a decisive factor for determining the properties and potential sites associated to the reactivity in biological systems and processes. In the mapping of electrostatic potential surface of **L^1**, the occurrence of negative potential in is found to be concentrated over the amide oxygen whereas the positive potential is around the amide proton. The MESP surfaces of complexes **1a-1c** (Fig. 7). (Red and blue colour symbolizes localization of negative and positive potential respectively) reveals the localization of positive potential around the metal centre in complex **1a** while in **1b** and **1c** negative potential is localized over the metal centres.

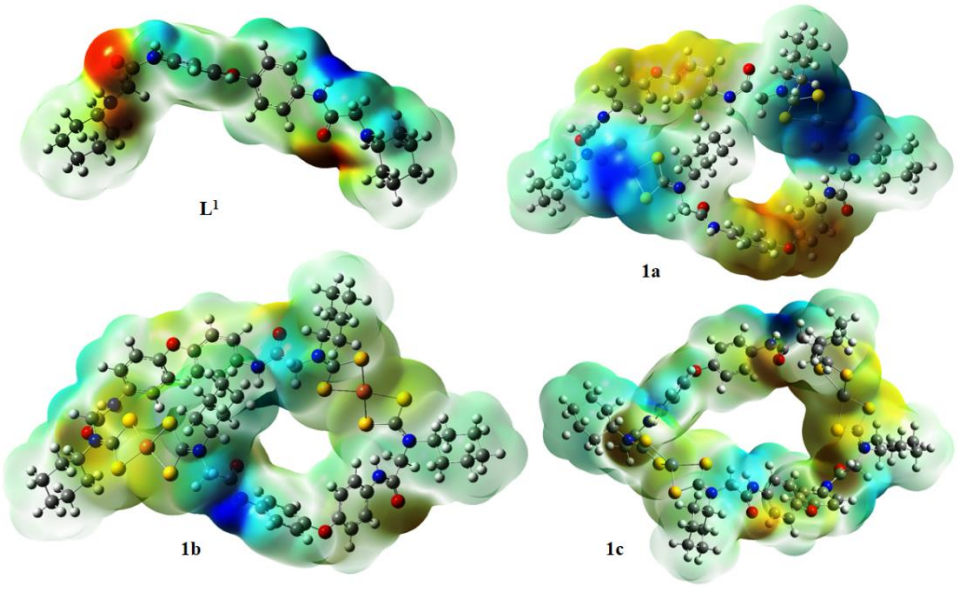

Fig.7. Depictions of electron density from total SCF density (Isovalue= 0.0004; mapped with ESP).

The molecular electrostatic potential of **1a-1c** clearly demonstrates the arrangement of the polar amide subunits towards the peripheral side of the macrocyclic motifs which further assists significant H-bond donor-acceptor sites to facilitate the interactions with biomolecules thus validating the excellent antitumor activity of these compounds on Hep G2 cell line.

5.3.6. *In vitro* cytotoxic activity

The lead compound 4, 4'- oxydianilne and all of its derivatives (**L'**, **L^1-L^3**, **1a-1c**, **2a-2c** and **3a-3c**) where screened for their effective *In vitro* cytotoxic activity by MTT assay against the malignant tumor cell line HepG2 (Hepatoma). Hep G2 cell line was carefully chosen because liver has the capacity to detoxify, metabolize inactivate exogenous compounds such as drugs, other exogenous and also endogenous compounds like steroids and it is commonly used as a model system for studies of liver metabolism and xenobiotics toxicity.[25] The cytotoxicity observed for these compounds were compared with the clinically used antineoplastic drug cisplatin [C]. The 50% inhibition concentration (IC50) values obtained after incubation for 24hrs for all the compounds

against HepG2 cell line are summarized in Table 4 and Fig. 8. Overall data suggest that all the compounds viz. **L^1**, **1a**, **1c**, **L^2**, **2a**, **2b**, **2c**, **L^3**, **3a**, **3b** and **3c** except **1b** exhibit better cytotoxicity than Cisplatin (75.67 ± 0.25 μM) and thus these were tested further on normal liver cell line (WRL-68) under similar conditions. The specificity of these newly synthesized compounds for cancer cells over normal liver cells can be clearly visualized from the experimental data summarized in Table 4. In particular, the first derivative **L'** of the lead compound 4,4'-diamino oxydianiline does not exhibit marked cytotoxicity against HepG2, however its diamino derivatives **L^1** (IC 50: 24.53 ± 0.13 μM), **L^2** (IC50: 8.68 ± 0.06 μM) and **L^3** (IC50: 5.49 ± 0.04 μM) exhibited remarkable cytotoxic effect in HepG2 cell line. Interestingly, the cytotoxic activity of **L^1-L^3** is further augmented in their corresponding complexes viz. **1a** (IC50: 7.27 ± 0.16 μM), **2c** (IC50: 3.55 ± 0.06 μM), **3a** (IC50: 4.42 ± 0.06 μM) and **3c** (IC50: 2.19 ± 0.04 μM). Notably, the activity of **L^1-L^3** falls down significantly upon the formation of corresponding nickel dithiocarbamate complexes **1b**, **2b** and **3b**. In general, 4,4'-bis(2-(n-butylamino)acetamido)biphenylether (**L^3**) holding *N*-Bu^n substituents showed the finest cytotoxicity (IC50= 5.49 μM) compared to **L^1** and **L^2** and this enhanced activity was further improved in metal bound dithiocarbamate derivatives **3a** and **3c**. Outstandingly, zinc complexes **2c** and **3c** demonstrate 21 folds to 34 folds better cytotoxic activity whereas **L^3**, **1a** and **3a** showed more than 10 fold better cytotoxic activity as compared to the reference drug Cisplatin (IC50: 75.67 ± 0.25 μM) against Hep G2 cell line. The enormous cytotoxicity of these derivatives against HepG2 cell line provides a strong background to investigate them further against other carcinoma human cell types in future.

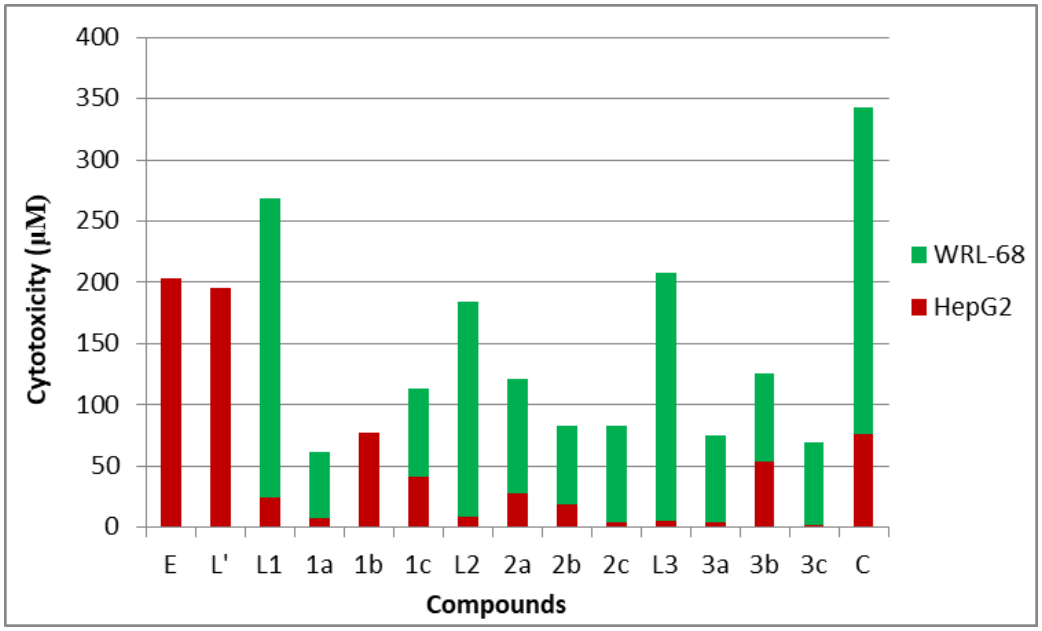

Fig. 8. Cytotoxic activity IC_{50} values (µM) for **L** and its derivatives E, **L'**, **L^1-L^3**, **1a-1c**, **2a-2c** and **3a-3c**.

Table 4
IC_{50} values for entry **1-15** against HepG2 cancer cells.

Entry	Compounds	Cytotoxicity IC50 µM ± SE	
		Hep G2	**WRL-68**
1	4,4'-diamino oxydianiline (**E**)	203.41 ± 0.13	-
2	4,4'-bis(2-chloroacetamido)diphenylether (**L'**)	195.87 ± 0.19	-
3	4,4'-bis(2-(cyclohexylamino)acetamido)diphenylether (**L^1**)	24.53 ± 0.13	244.46 ± 0.21
4	4,4'-bis(2-(isopropylamino)acetamido)diphenylether (**L^2**)	8.68 ± 0.06	175.96 ± 0.34
5	4,4'-bis(2-(n-butylamino)acetamido)biphenylether (**L^3**)	5.49 ± 0.04	202.15 ± 0.18
6	[Ni_2-μ^2-bis-{(κ^2S,S-$S_2CN(Cy)CH_2CONHC_6H_4)_2O$}] (**1a**)	7.27 ± 0.16	54.07 ± 0.35
7	[Cu_2-μ^2-bis-{(κ^2S,S-$S_2CN(Cy)CH_2CONHC_6H_4)_2$ O }] (**1b**)	77.37 ± 0.25	-
8	[Zn_2-μ^2-bis-{(κ^2S,S-$S_2CN(Cy)CH_2CONHC_6H_4)_2$ O }] (**1c**)	41.44 ± 0.29	71.41 ± 0.25
9	[Ni_2-μ^2-bis-{(κ^2S,S-$S_2CN(^iPr)CH_2CONHC_6H_4)_2$ O }] (**2a**)	27.25 ± 0.18	93.67 ± 0.41
10	[Cu_2-μ^2-bis-{(κ^2S,S-$S_2CN(^iPr)CH_2CONHC_6H_4)_2$ O }] (**2b**)	19.14 ± 0.17	64.18 ± 0.48
11	[Zn_2-μ^2-bis-{(κ^2S,S-$S_2CN(^iPr)CH_2CONHC_6H_4)_2$ O }] (**2c**)	3.55 ± 0.06	79.65 ± 0.26
12	[Ni_2-μ^2-bis-{(κ^2S,S-$S_2CN(^nBu)CH_2CONHC_6H_4)_2$ O }] (**3a**)	4.42 ± 0.06	71.07 ± 0.36
13	[Cu_2-μ^2-bis-{(κ^2S,S-$S_2CN(^nBu)CH_2CONHC_6H_4)_2$ O }] (**3b**)	54.02 ± 0.07	71.73 ± 0.48
14	[Zn_2-μ^2-bis-{(κ^2S,S-$S_2CN(^nBu)CH_2CONHC_6H_4)_2$ O }] (**3c**)	2.19 ± 0.04	67.64 ± 0.20
15	Cisplatin (**C**)	75.67 ± 0.25	

The efficacy of cytotoxic drugs is measured by their ability to selectively promote apoptosis in cancer cells while causing less or no damage to normal healthy cells[41, 42] as observed in our study where complexes showing IC_{50} lower than Cisplatin (**L^1**, **1a**, **1c**, **L^2**, **2a**, **2b**, **2c**, **L^3**, **3a**, **3b** and **3c**) selectively targeted cancerous cells HepG2 and incurred little or no death in normal liver cell line WRL-68. Apoptosis induction is a key event and a preferred pathway for induction of cell death. Apoptosis is a regulated programmed cell death which controls both the rate of cell division as well as that of cell death and regulates several functions of the body, such as development of cell population in tissues, regulating immune system and aging, and many more. A characteristic apoptotic sign is the shrinking of cells,[43] a mechanism of the action of our test compounds can be visualized by phase contrast images (Fig. 9) and more clearly by acridine orange/ethidium bromide (AO/EB) staining which differentiates between viable, apoptotic and necrotic cells and marks nuclear changes (Fig. 10).

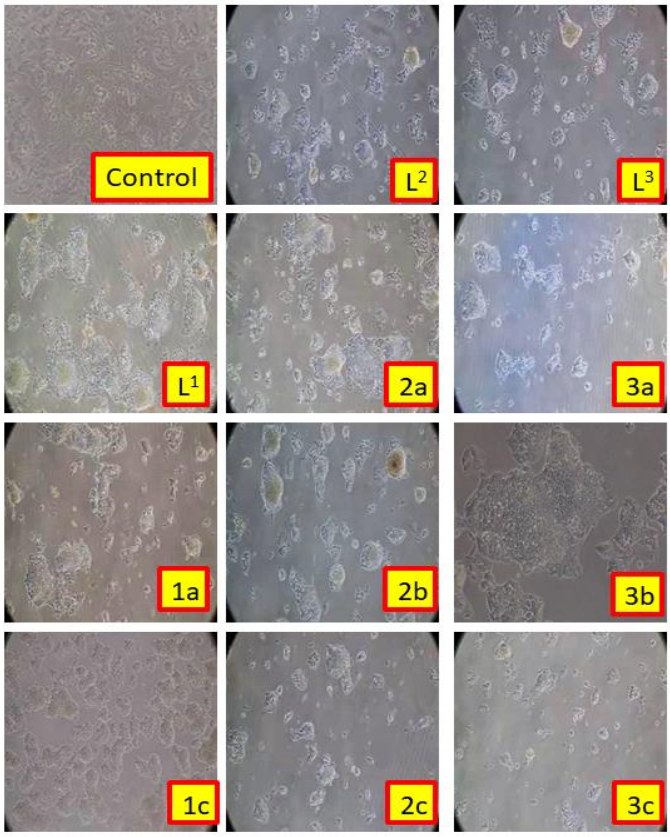

Fig. 9. Phase Contrast images of Hep G2 cells exposed to the potential compounds **L^1-L^3**, **1a**, **1c**, **2a-2c** and **3a-3c** compared to the control indicating the *in-vitro* cytotoxic activity. These compounds were assayed at their respective *in-vitro* growth inhibitory IC_{50} value, as determined using the MTT assay in Hep G2 cells.

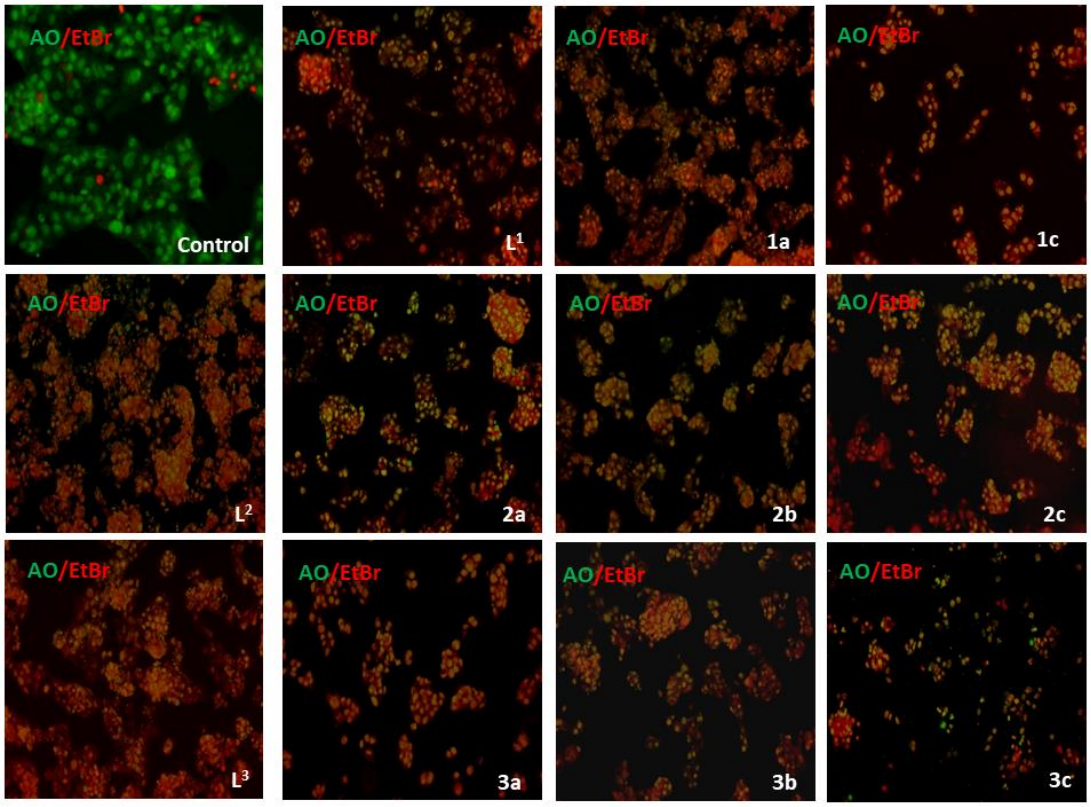

Fig. 10. Acridine Orange (AO)-Ethidium Bromide (EB) staining for detection of live and Apoptotic cells-Green denotes live cells with AO stained cells while red dented apoptotic cells stained with EB

Complexes- **L^1**, **1a**, **1c**, **L^2**, **2a**, **2b**, **2c**, **L^3**, **3a**, **3b** and **3c** were stained for AO/EB where viable cells are stained by AO and show green fluorescence whereas apoptotic cells are stained by EB and show orange to red fluorescence with condensed chromatin.[44] These observations encourage us to work further to elucidate the exact mechanism and pathway of apoptosis being followed.

5.4. Conclusion

Furtherance to our ongoing research interest in synthesizing probable metal-based drugs,[14, 18, 19] demonstrating significant cytotoxic activity and also based on the observation of tumour-inhibiting property of 4,4'-oxydianiline in mice,[11, 12] we have prepared a number of derivatives of 4,4'-oxydianiline viz **L'**, **L^1-L^3** and their metal bound dithiocarbamate derivatives (vide supra). All these compounds were structurally characterized by FT-IR, MS, ^{1}H, ^{13}C, ^{1}H DOSY NMR spectroscopy, UV-visible, fluorescence spectrophotometers and by thermogravimetric analysis and these were further supported by DFT level calculations. MTT assay was carried out on all the compounds to explore for their *in vitro* cytotoxic activity against malignant human tumor Hep G2 (hepatoma) cell line. The first derivative of 4,4'-oxydianiline **L'** didn't show any marked cytotoxicity, however its diamino derivatives **L^1-L^3** in their metal-free form and metallomacrocyclic complexes, **1a**, **1c**, **2a**, **2b**, **2c**, **3a**, **3b** and **3c** exhibit higher cytotoxicity than Cisplatin. Specifically, **L^2** (8.68 ± 0.06 µM), **L^3** (5.49 ± 0.04µM), **1a** (7.27 ± 0.16 µM), **2c** (3.55 ± 0.06µM), **3a** (4.42 ± 0.06 µM) and **3c** (2.19 ± 0.04 µM) shows more than 10 fold better cytotoxic activity and 37 fold in case of **3c** against Hep G2 cell line, compared to the reference drug Cisplatin. Outstanding cytotoxic activity of many of the derivatives opens the scope for further investigations against other carcinoma human cell types. Morphological evidences like shrinking of cells indicates the induction of apoptosis as part of the mechanism of action of these compounds which is further supported by the distinct staining of the cells by acridine orange/ethidium bromide (AO/EB). Nevertheless, further investigation is required to explicate the thorough mechanism and pathway of apoptosis.

5.5 References

[1] R. T. Chern, W. J. Koros, B. Yui, H. B. Hopfenberg, V. T. Stannett, *J. Polym. Sci. Part B* **1984**, *22*, 1061-1084.

[2] T. H. Kim, W. J. Koros, G. R. Husk, K. C. O'Brien, *J. Membr. Sci.* **1988**, *37*, 45-62.

[3] K. Okamoto, K. Tanaka, H. Kita, A. Nakamura, Y. Kusuki, *J. Polym. Sci, Part B* **1989**, *27*, 1221-1233.

[4] K. Tanaka, H. Kita, K. Okamoto, A. Nakamura,Y. Kusuki, *J . Membr. Sci*. 1989, *47*, 203-215.

[5] M. R. Coleman, W. J. Koros, *J. Membr. Sci.* **1990**, *50*, 285-297.

[6] H. C. W. M. Buys, A. Van Eleven, A. E. Jansen, A. H. A. Tinnemans, *J. Appl. Polym.Sci*. **1990**, *41*, 1261-1270.

[7] K. Kneifel, K. V. Peinemann, *J. Membr. Sci*. **1992**, *65*, 295-307.

[8] S. Tamai, T. Kuroki, A. Shibuya, A. Yamaguchi, *Polymer* **2001**, *42*, 2373–2378.

[9] J. G. Clabes, M. J. Goldberg, A. Viehbeck, C. A. Kovac, *J. Vac. Sci. Technol*. **1988**, *6*, 985-991.

[10] E. K. Weisburger, A. S. K. Murthy, H. S. Lilja, J. C. Lamb, *National Cancer Institute* **1984**, *72*, 1457-1464.

[11] E. Boyland, *Biochem. J*. **1946**, *40*, 55-58.

[12] K. Tanaka, T. Ino, T. Sawakata, S. Marui, H. Igaki, H. Yashima, *Mutat. Res*. **1985**, *143*, 11-15.

[13] V. K. Singh, R. Kadu, H. Roy, *Eur. J. Med. Chem*. **2014**, *74*, 552-561.

[14] R. Kadu, H. Roy, V. K. Singh, *Appl. Organomet. Chem.* **2015**, *29*, 746-755.

[15] E. M. Driggers, S. P. Hale, J. Lee, N. K. Terrett, *Nat. Rev. Drug Discov*. **2008**, *7*, 608-624.

[16] J. Mallinson and I. Collins, *Future Med Chem* . **2012**, *4*, 1409-1438.

[17] A. Mann, Wermuth CG (Ed.) Academic Press, London, UK **2008**.

[18] V. K. Singh, R. Kadu, H. Roy, P. Raghavaiah, S. M. Mobin, *Dalton Trans.* **2015**, *45*, 1443-1454.

[19] V. Pillai, R. Kadu, L. Buch, V. K. Singh, *ChemistrySelect* **2017**, *2*, 4382-4391.

[20] A. Alama, B. Tasso, F. Novelli, F. Sparatore, *Drug Discov. Today* **2009**, *14*, 500-508.

[21] A. Kamal, B. A. Kumar, M. Arifuddin, S. G. Dastidar, *Bioorg. Med. Chem*. **2003**, *11*, 5135-5142.

[22] Y. Singh, M. Palombo, P. J. Sinko, *Curr. Med. Chem*. **2008**, *15*, 1802-1826.

[23] G. Faraglia, D. Fregona, S. Sitran, L. Giovagnini, C. Marzano, F. Baccichetti, U. Casellato, R. Graziani, *J. Inorg. Biochem*. **2001**, *83*, 31-40.

[24] R. Kieltyka, P. Englebienne, J. Fakhoury, C. Autexier, N. Moitessier, H. F. Sleiman, *J. Am. Chem. Soc*. **2008**, *130*, 10040-10041.

[25] V. Mersch-Sundermann, S. Knasmüller, X. J. Wu, F. Darroudi, F. Kassie, *Toxicology* **2004**, *198*, 329–340.

[26] S. K. Verma, V. K. Singh, *J. Organomet. Chem*. **2015**, *791*, 214-224.

[27] S. K. Verma, Vinay K. Singh, *J. Coord. Chem.* **2015**, *68*, 1072–1087.

[28] S. K. Verma, V. K. Singh, *RSC Adv*. **2015**, *5*, 53036-53046.

[29] S. Leininger, B. Olenyuk, P. J. Stang, *Chem. Rev*. **2000**, *100*, 853-908.

[30] C. J. Jones, *Chem. Soc. Rev*. **1998**, *27*, 289-299.

[31] R. Kadu, V. Pillai, V. Amrit, V. K. Singh, *RSC Adv*. **2015**, *5*, 106688-106699.

[32] M. D. Pratt, Paul D. Beer, *Tetrahedron*, **2004**, *60*, 11227-11238.

[33] S. K. Verma, R. Kadu, V. K. Singh, *Synth. React. Inorg. Met.-Org. Nano-Met. Chem*. **2014**, *44*, 441–448.

[34] Y. Yan, S. Krishnakumar, H. Yu, S. Ramishetti, Lih-Wen Deng, S. Wang, L. Huang, D. Huang, *J. Am. Chem. Soc*. **2013**, *135*, 5312-5315.

[35] H. H. Wasserman, R. W. Murray. Singlet oxygen. New York: Academic Press, **1979**.

[36] S. Leininger, B. Olenyuk, P. J. Stang, *Chem. Rev*. **2000**, *100*, 853-908.

[37] M. J. Frisch, G. W. Trucks, H. B. Schlegel, G. E. Scuseria, M. A. Robb, J. R. Cheeseman, J. A. Montgomery Jr., T. Vreven, K. N. Kudin, J. C. Burant, J. M. Millam, S. S. Iyengar, J. Tomasi, V. Barone, B. Mennucci, M. Cossi, G. Scalmani, N. Rega, G. A. Petersson, H. Nakatsuji, M. Hada, M. Ehara, K. Toyota, R. Fukuda, J. Hasegawa, M. Ishida, T. Nakajima, Y. Honda, O. Kitao, H. Nakai, M. Klene, X. Li, J. E. Knox, H. P. Hratchian, J. B. Cross, C. Adamo, J. Jaramillo, R. Gomperts, R. E. Stratmann, O. Yazyev, A. J. Austin, R. Cammi, C. Pomelli, J. W. Ochterski, P. Y. Ayala, K. Morokuma, G. A. Voth, P. Salvador, J. J. Dannenberg, V. G. Zakrzewski, S. Dapprich, A. D. Daniels, M. C. Strain, O. Farkas, D. K. Malick, A. D. Rabuck, K. Raghavachari, J. B. Foresman, J. V. Ortiz, Q. Cui, A. G. Baboul, S. Clifford, J. Cioslowski, B. B. Stefanov, G. Liu, A. Liashenko, P. Piskorz, I. Komaromi, R. L. Martin, D. J. Fox, T. Keith, M. A. A.-Laham, C. Y. Peng, A. Nanayakkara, M. Challacombe, P. M. W. Gill, B. Johnson, W. Chen, M. W. Wong, C. Gonzalez and J. A. Pople, Gaussian, Inc., Wallingford, CT, **2004**.

[38] D. Ghosh, K. Sen, A. K. Das, *Struct Chem*. **2012**, *23*, 227-235; X. Yu, N. Wang, H. He, L. Wang, *SpectrochimActa A*, **2014**, *122*, 283-287; M. Dolores Palacios, M. C. Puerta, P. Valerga, A.Lledos, E. Veilly, *Inorg. Chem*. **2007**, *46*, 6958-6967.

[39] (a) P. D. Beer, A. G. Cheetham, M. G. B. Drew, O. Danny Fox, J. Elizabeth Hayes, T. D. Rolls, *Dalton Trans*. **2003**, *4*, 603–611. (b) J. Cookson, E. A. L. Evans, J. P. Maher, C. J. Serpell, R. L. Paul, A. R. Cowley, M. G. B. Drew, P. D. Beer, *Inorg. Chim. Acta*, **2010**, *363*, 1195–1203. (c) Siu-Wai Lai, M. G. B. Drew, P. D. Beer, *J. Organomet. Chem*. **2001**, *637–639*, 89–93.

[40] R. Kadu, V. Pillai, V. Amrit and V. K. Singh, *RSC Adv*., 2015, **5,** 106688-106699.

[41] Green, Douglas. Means to an End: Apoptosis and other Cell Death Mechanisms. Cold Spring Harbor, NY: Cold Spring Harbor Laboratory Press, **2011**.

[42] A. K. Taraphdar, M. Roy, R. Bhattacharya, *Curr Sci*. **2001**, *80*, 1387–96.

[43] M. P. Mattson, *Brain Pathology* **2000**, *10*, 300-312.

[44] K. Liu, P. C. Liu, R. Liu, X. Wu, *Medical science monitor basic research* **2015**, *21*, 15-20.

5.6 Annexures:

5.6.1 Spectral characterization

Mass spectra

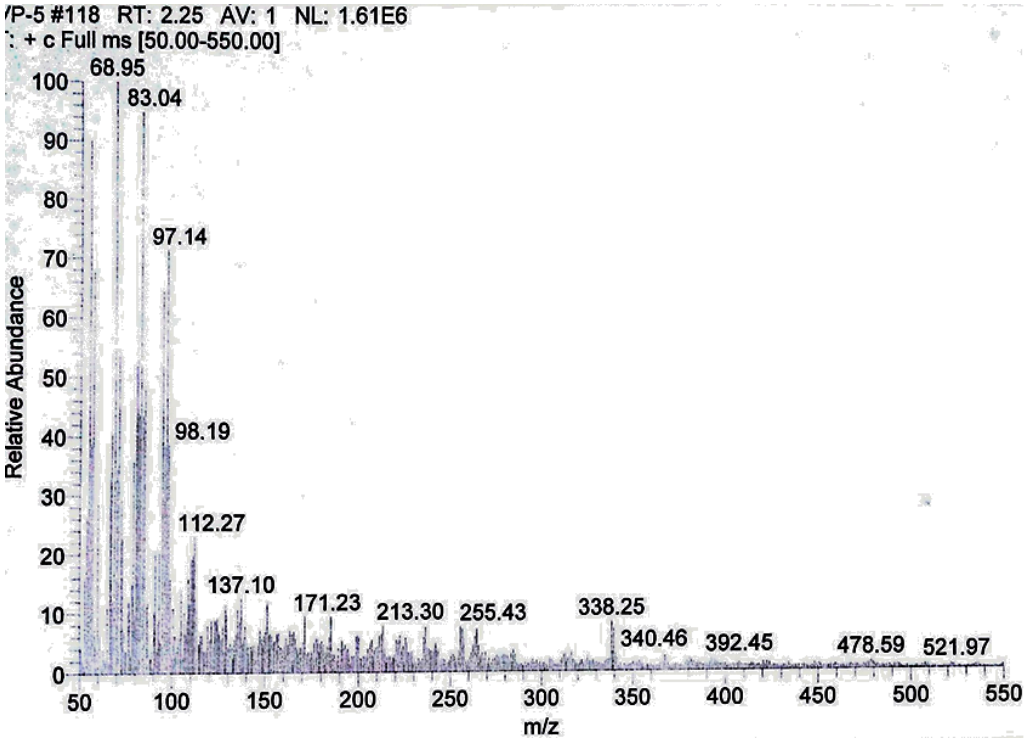

Annexure 1. Mass spectrum of L^1.

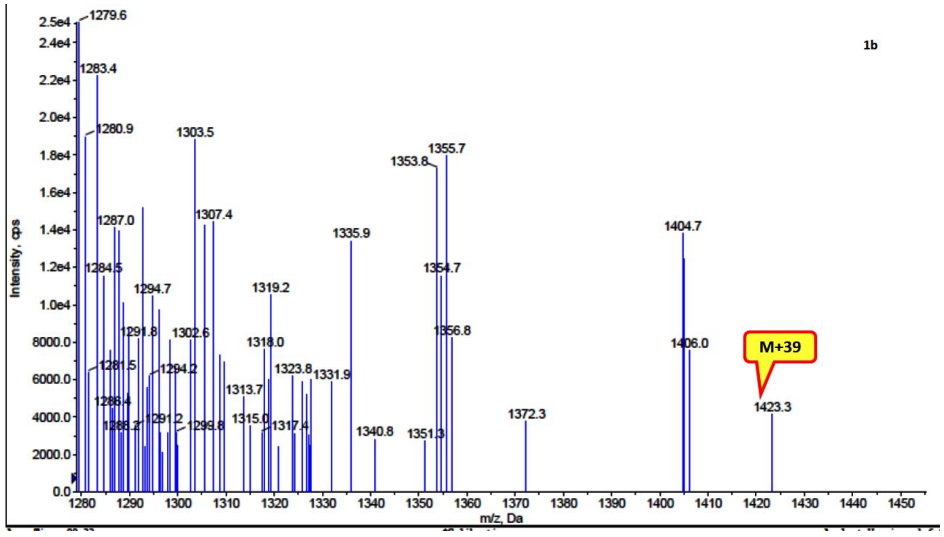

Annexure 2. Mass spectrum of 1b.

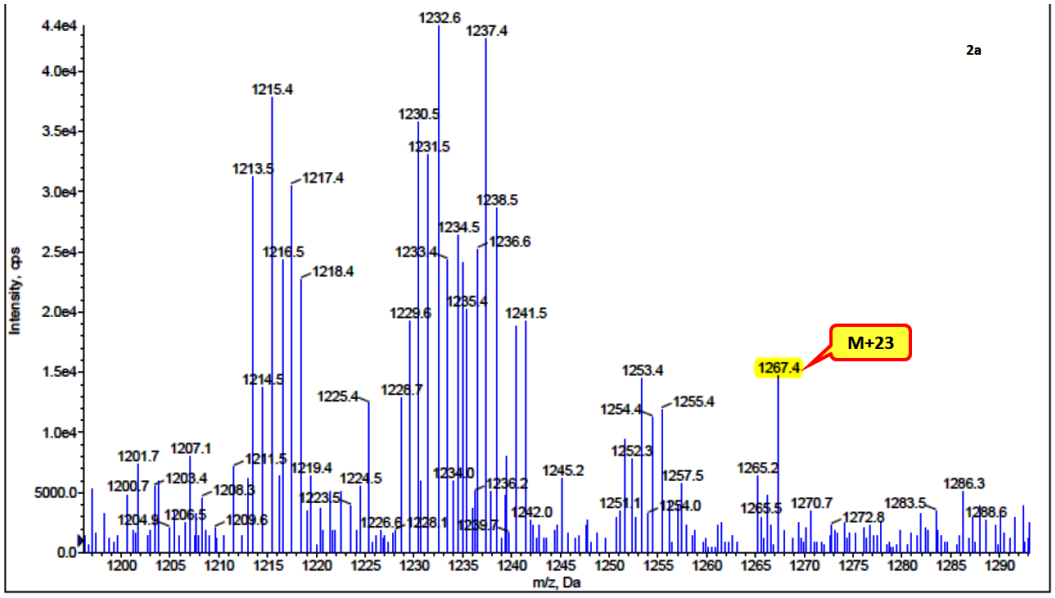

Annexure 3. Mass spectrum of 2a.

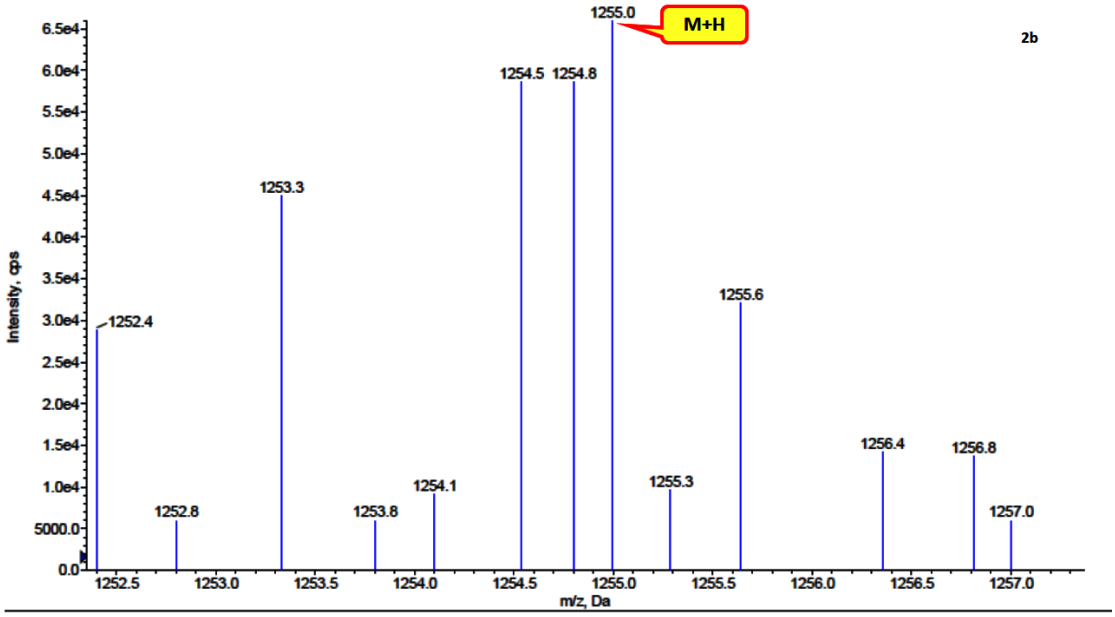

Annexure 4. Mass spectrum of 2b.

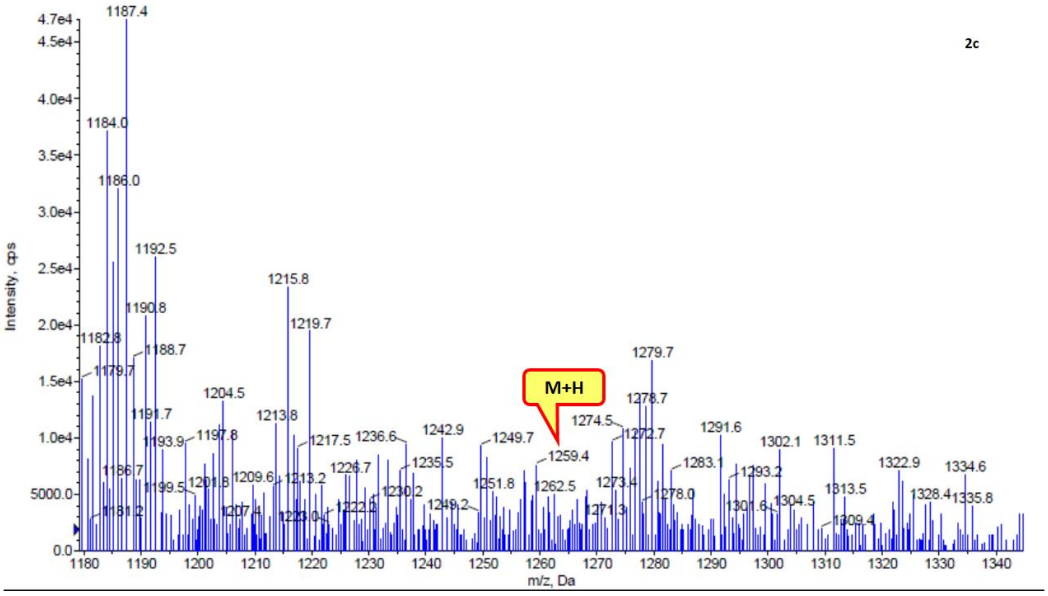

Annexure 5. Mass spectrum of 2c.

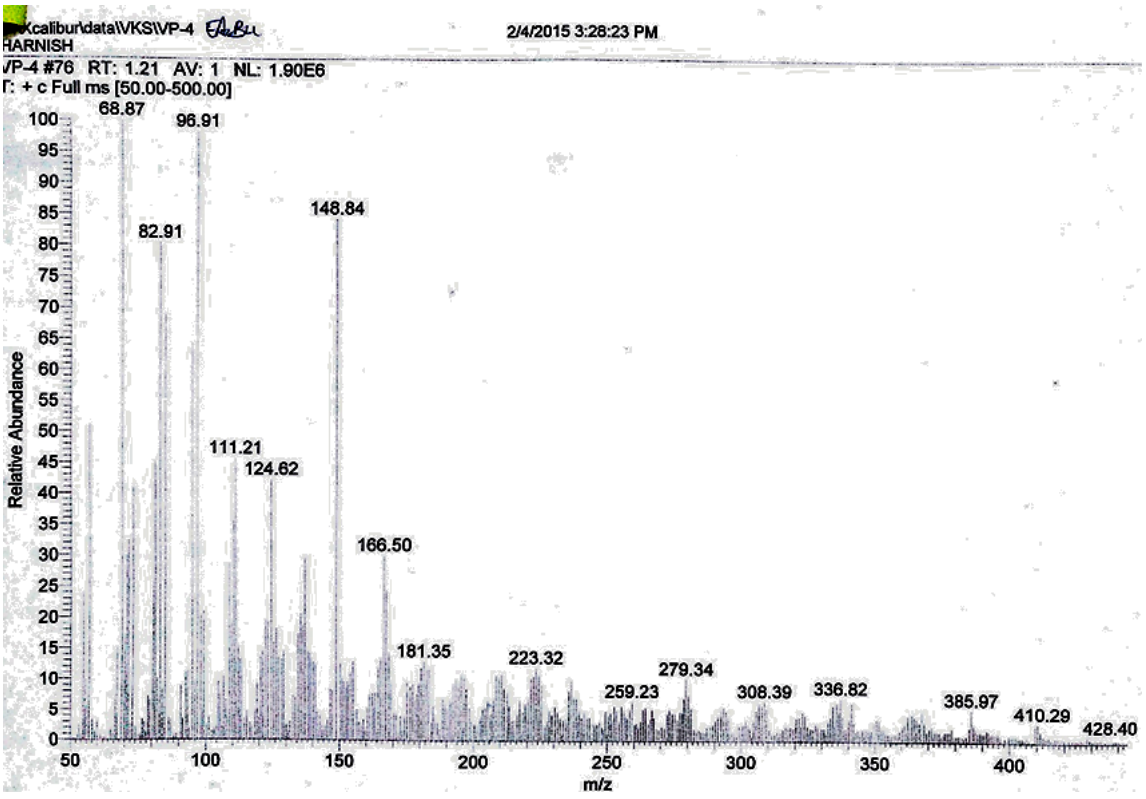

Annexure 6. Mass spectrum of L^3.

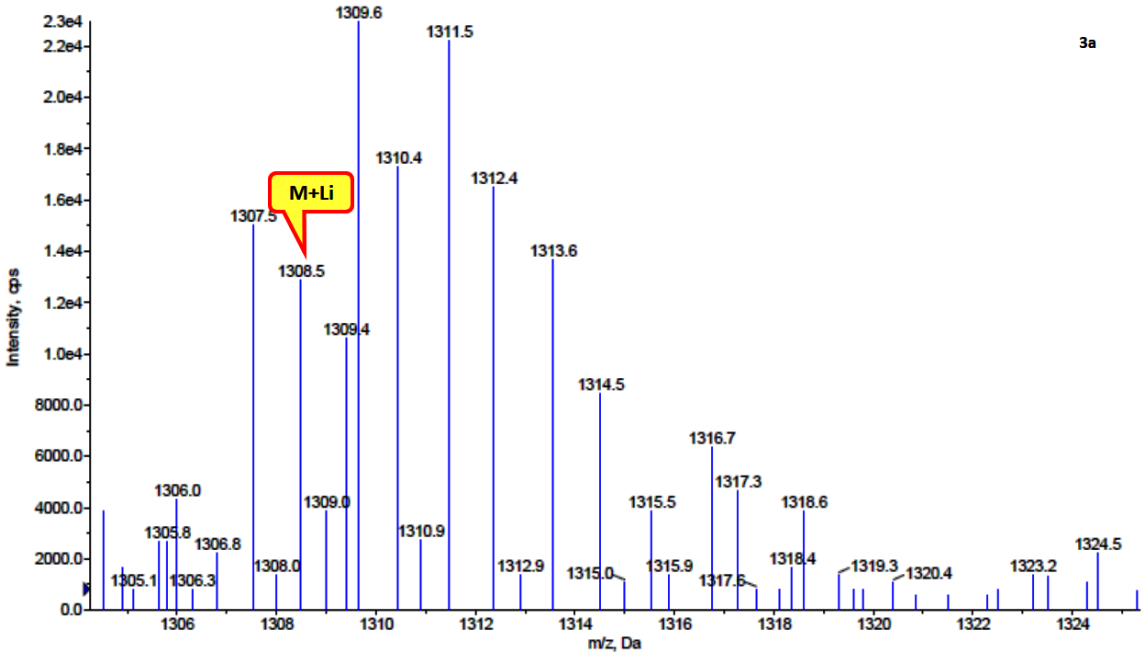

Annexure 7. Mass spectrum of 3a.

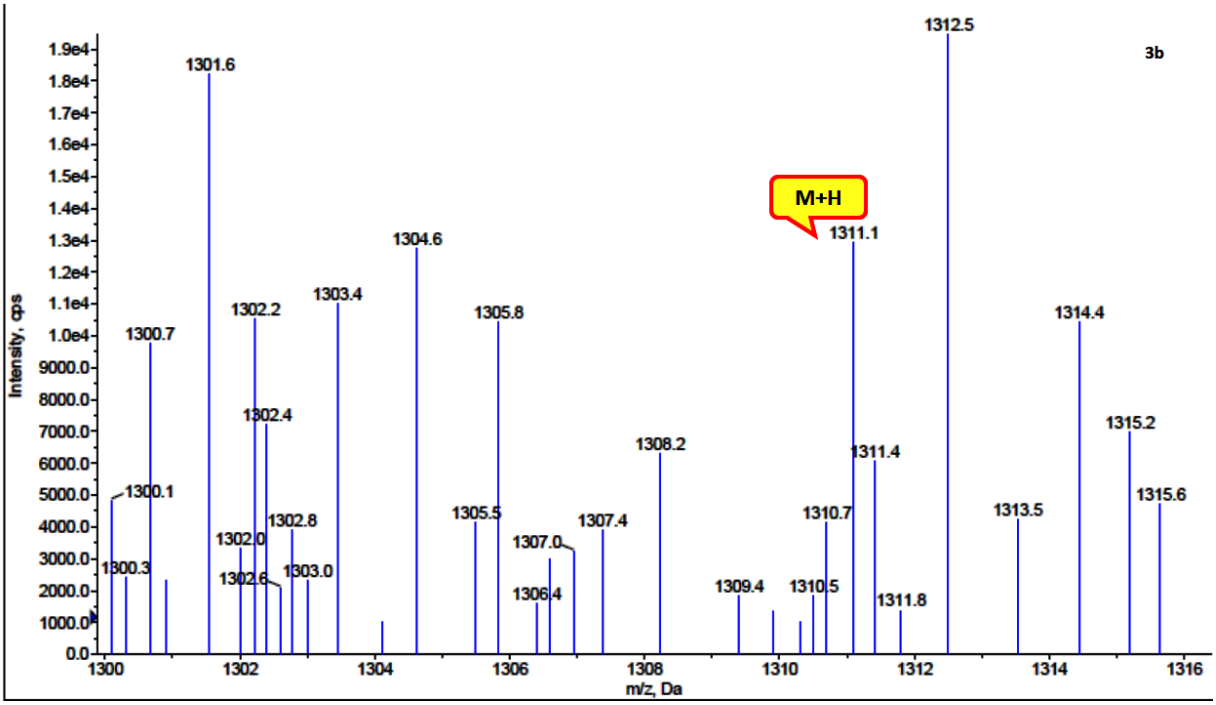

Annexure 8. Mass spectrum of 3b.

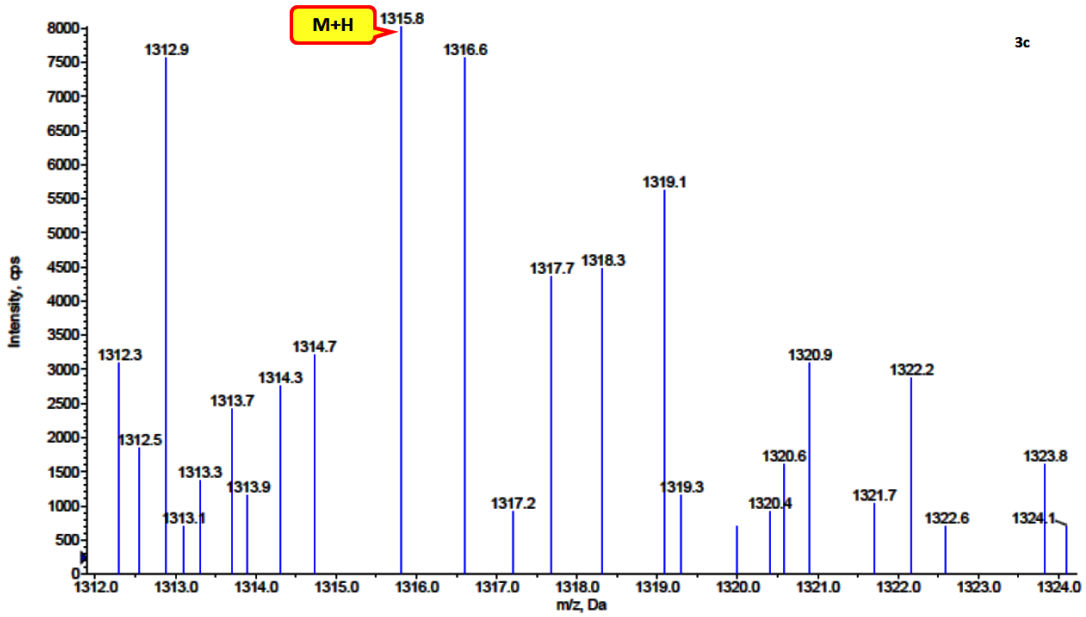

Annexure 9. Mass spectrum of 3c.

IR spectral data

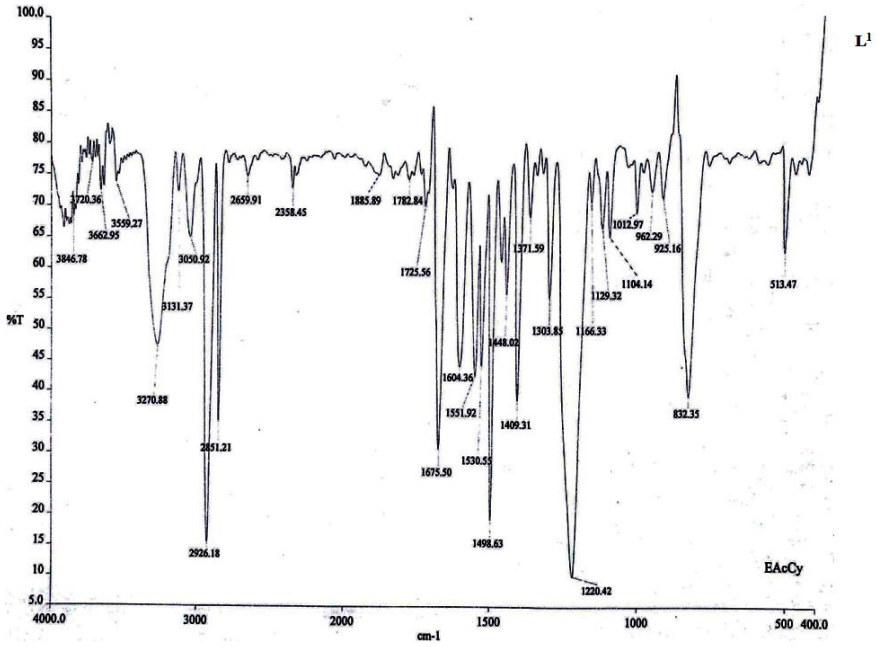

Annexure 10. IR spectrum of **L[1]**

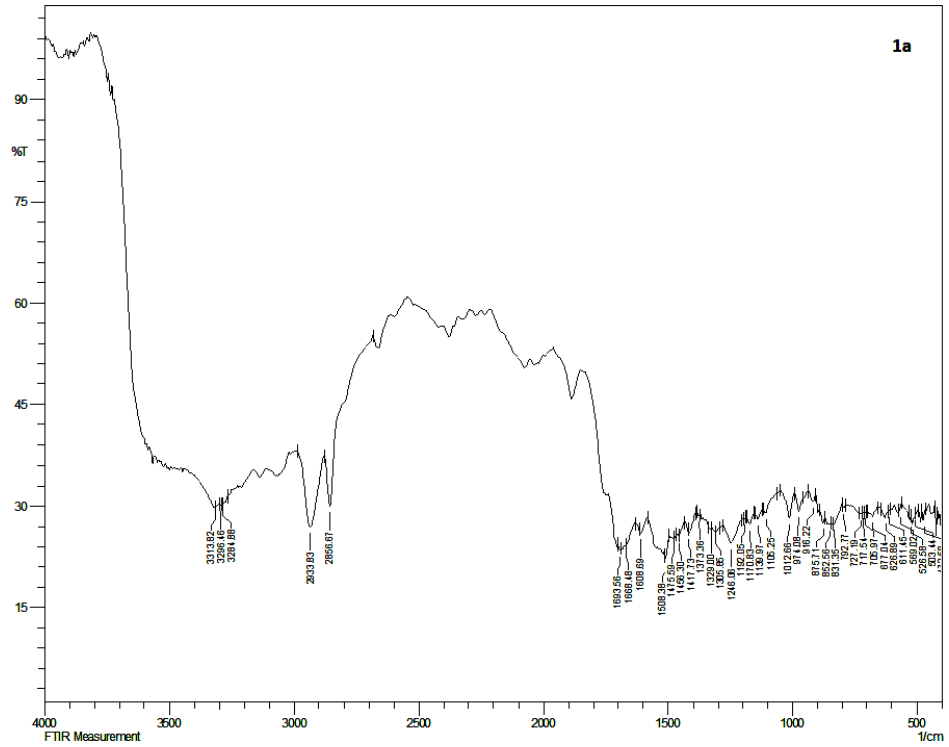

Annexure 11. IR spectrum of 1a

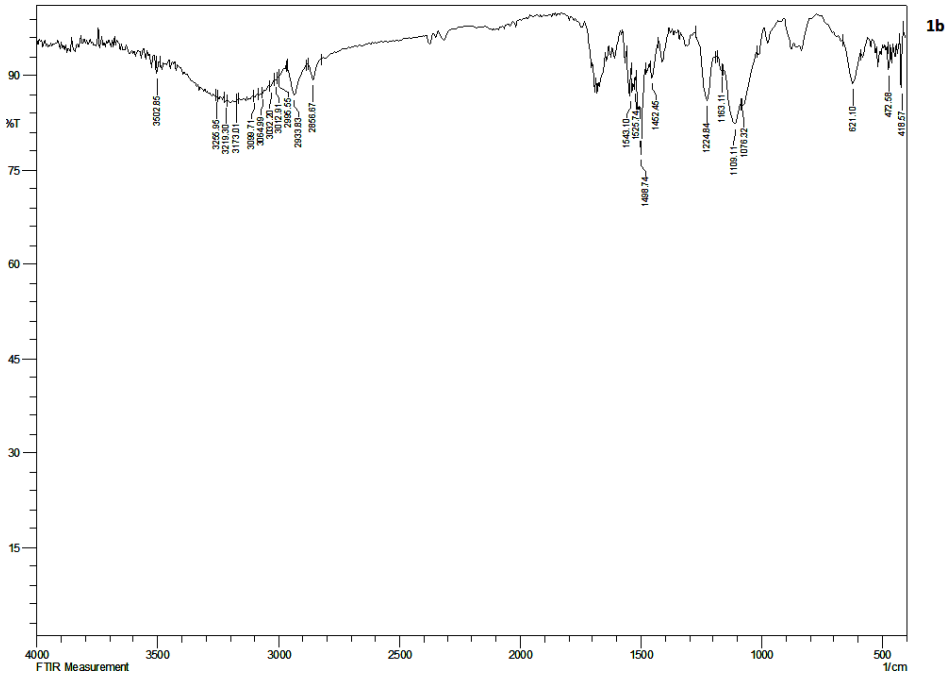

Annexure 12. IR spectrum of 1b

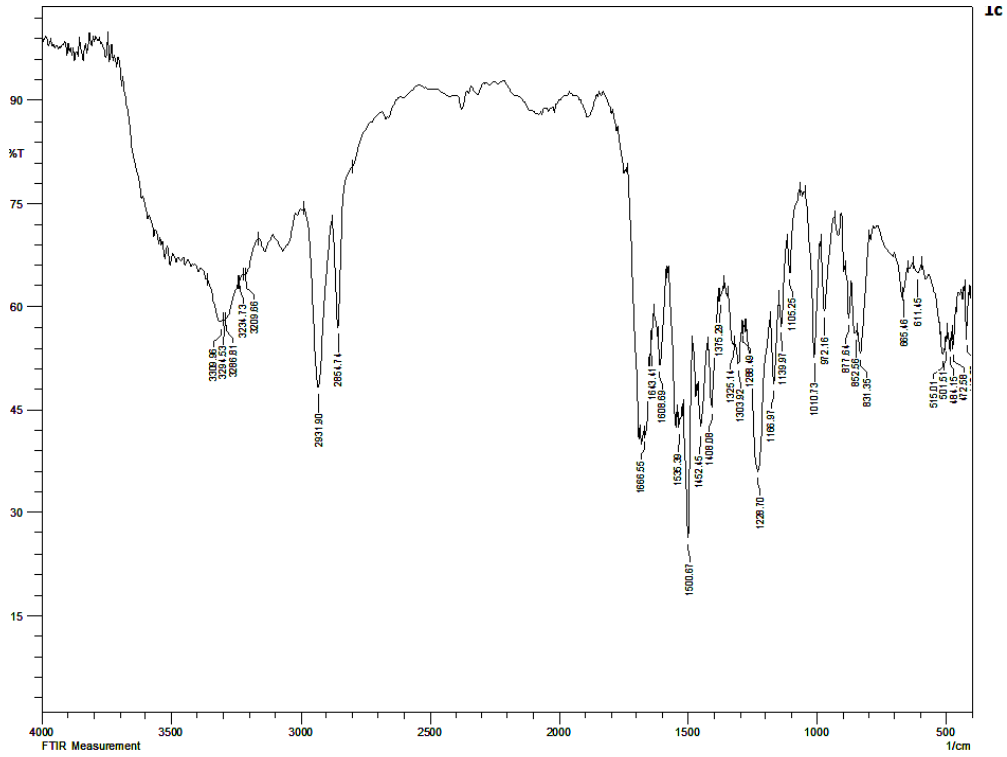

Annexure 13. IR spectrum of 1c

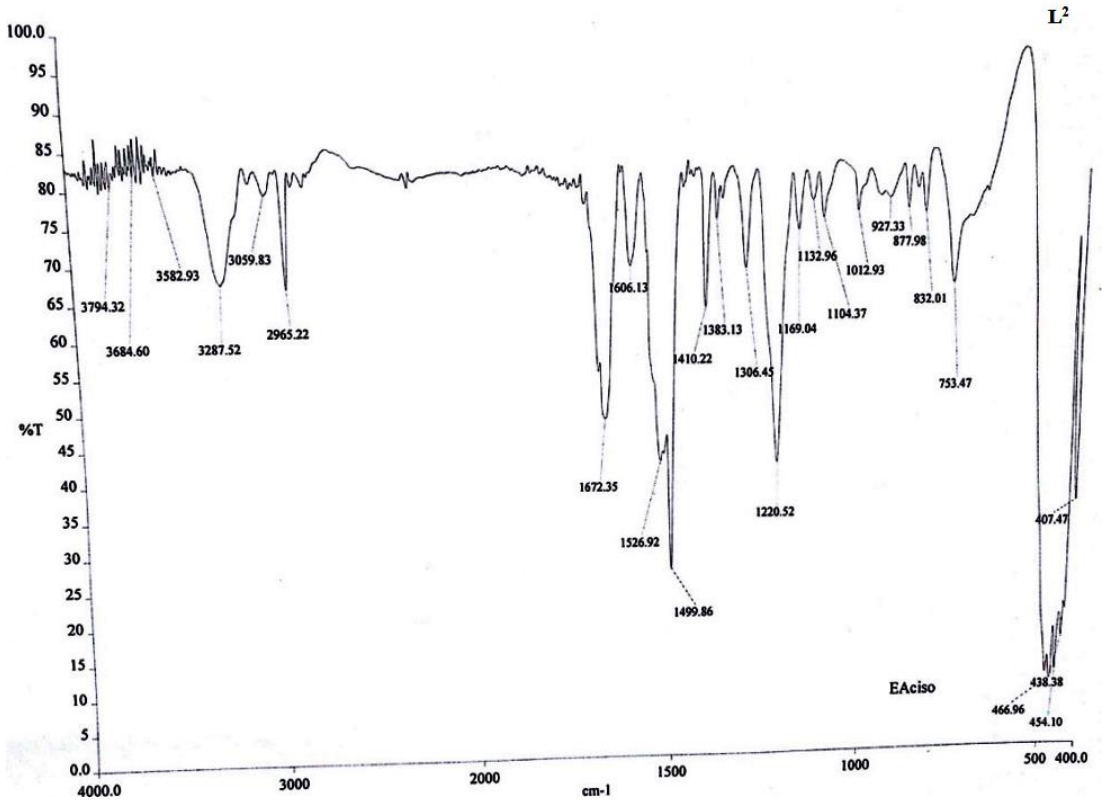

Annexure 14. IR spectrum of $\mathbf{L^2}$

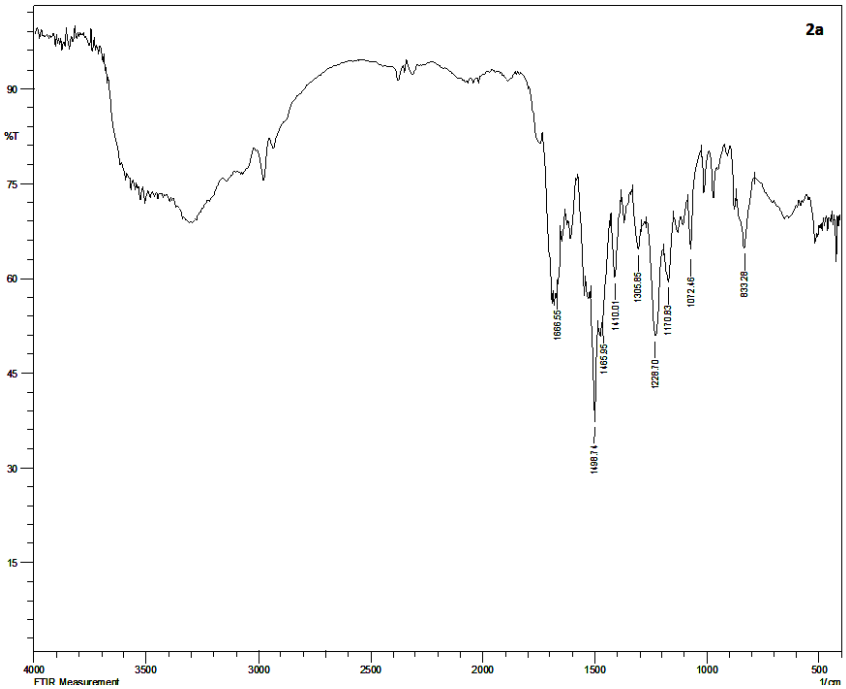

Annexure 15. IR spectrum of 2a

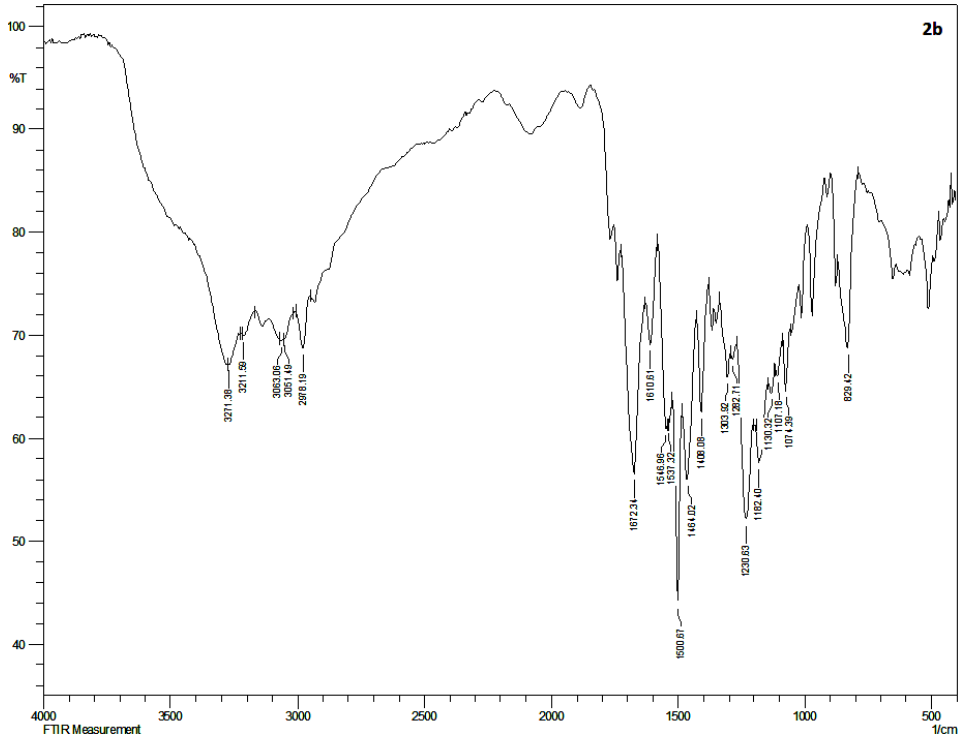

Annexure 16. IR spectrum of 2b

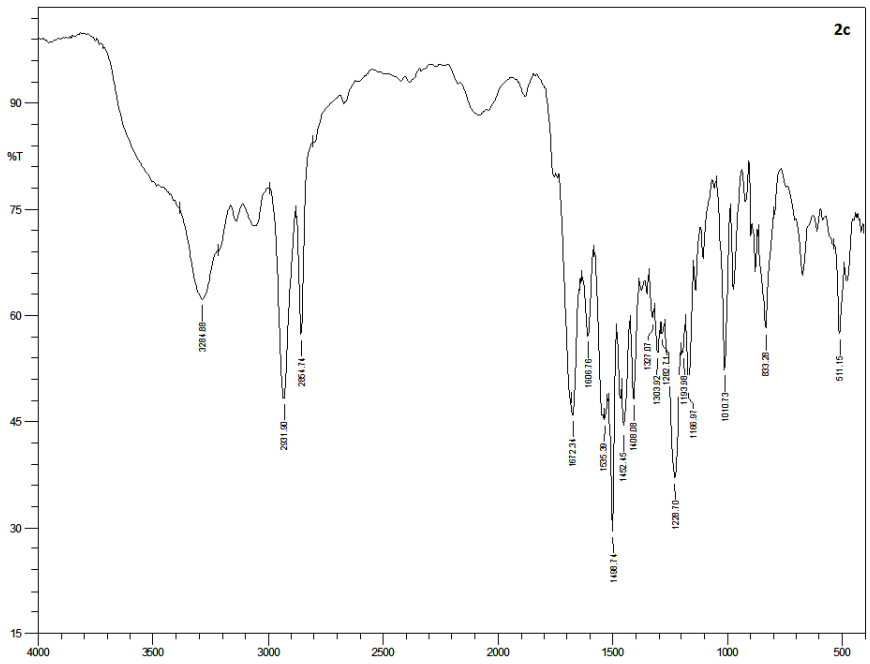

Annexure 17. IR spectrum of 2c

NMR spectral data

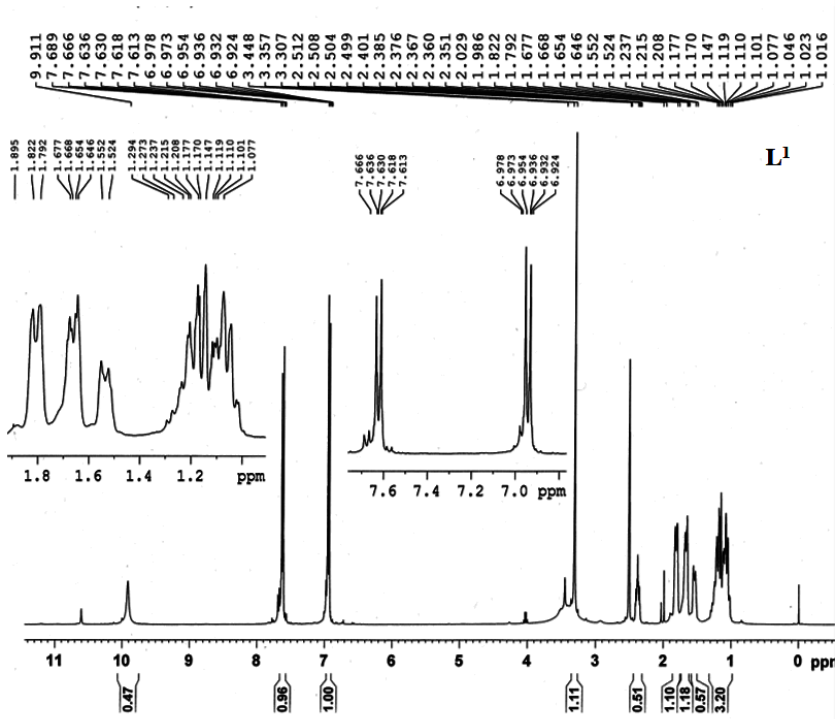

Annexure 18. ^{1}H NMR spectrum of **(L^1)**

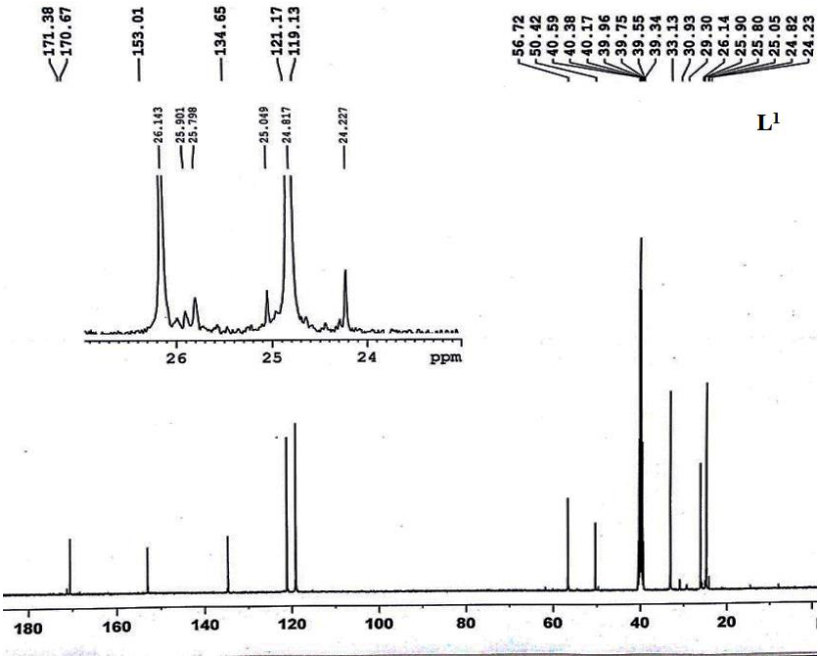

Annexure 19. ^{13}C NMR spectrum of **(L^1)**

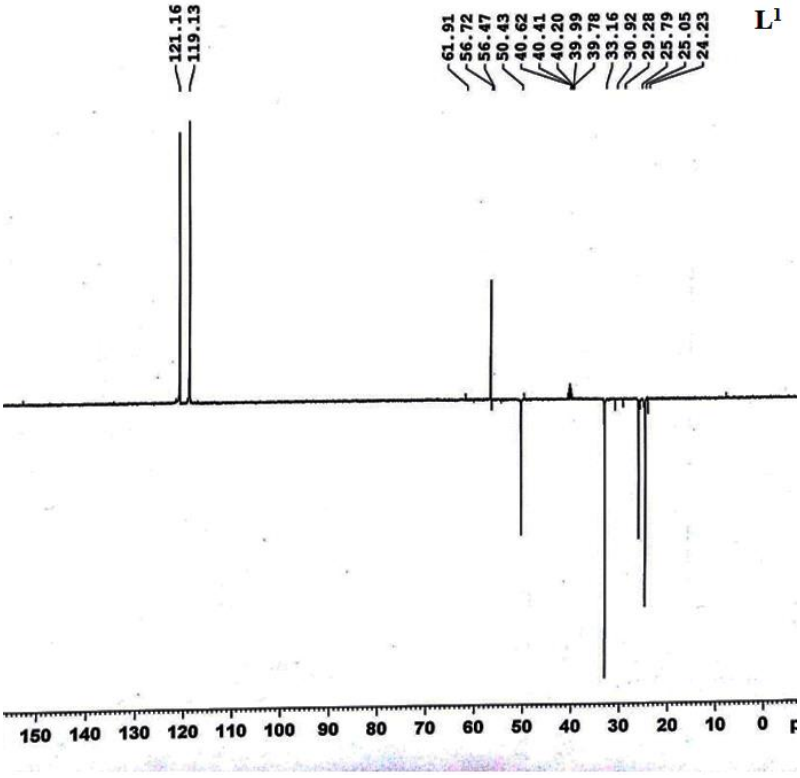

Annexure 20. DEPT-135 spectrum of **(L^1)**

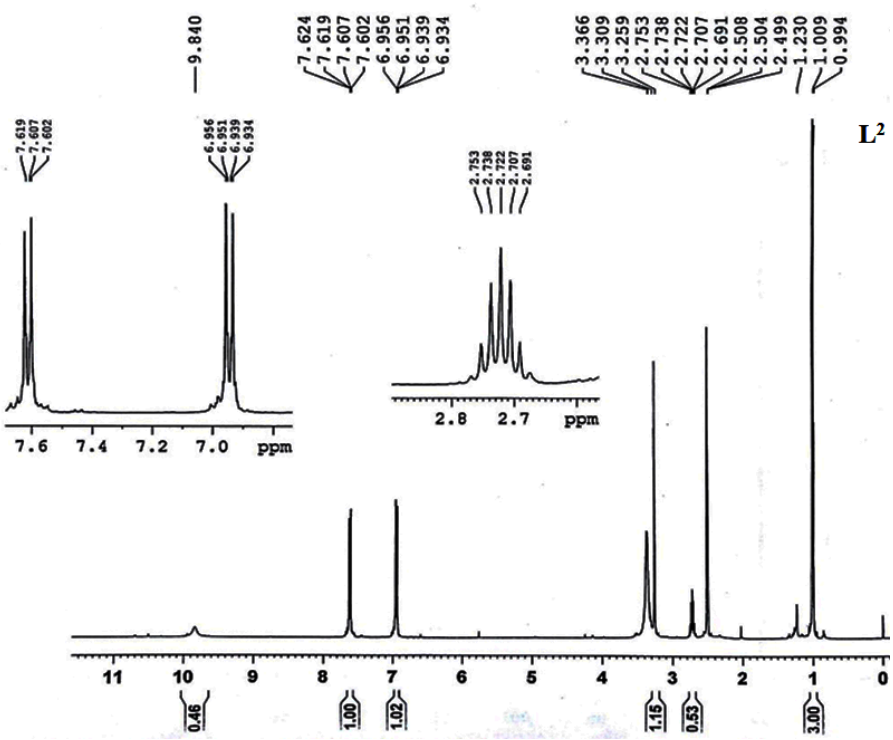

Annexure 21. ^{1}H NMR spectrum of **(L²)**

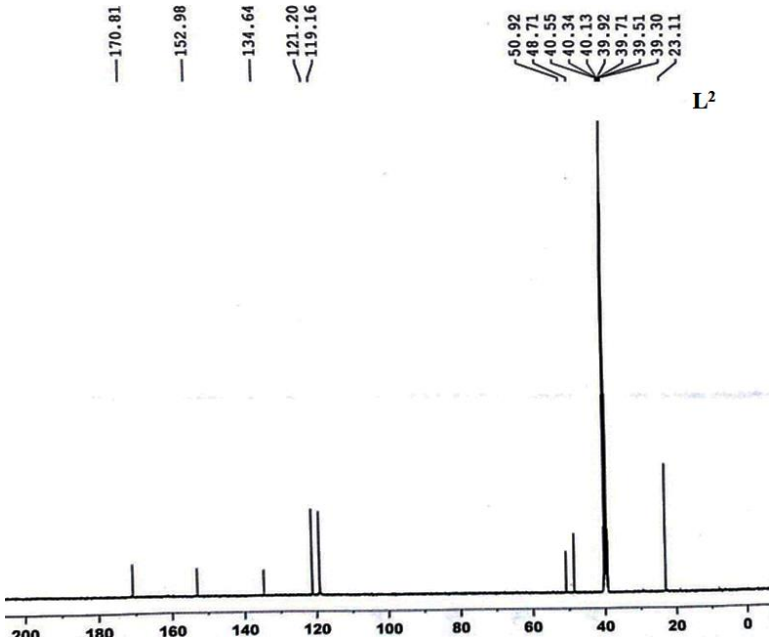

Annexure 22. ^{13}C NMR spectrum of **(L²)**

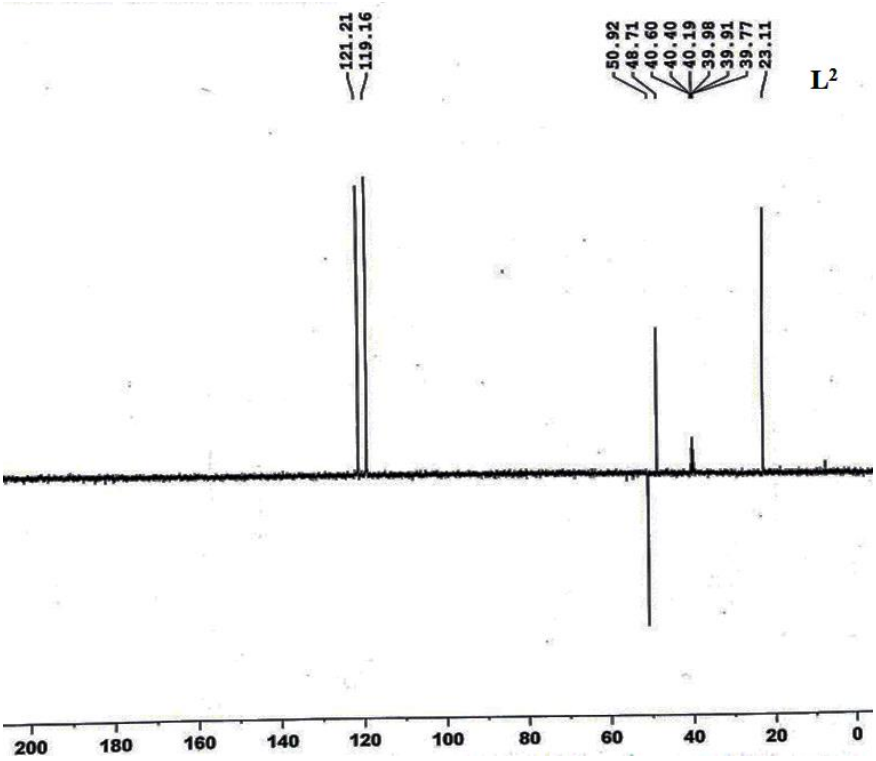

Annexure 23. DEPT-135 spectrum of **(L^2)**

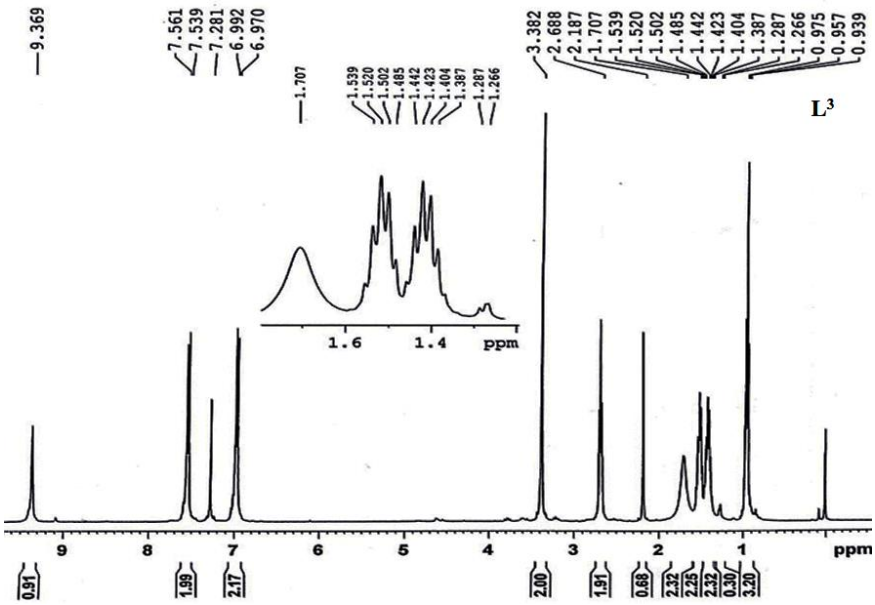

Annexure 24. ^{1}H NMR spectrum of **(L^3)**

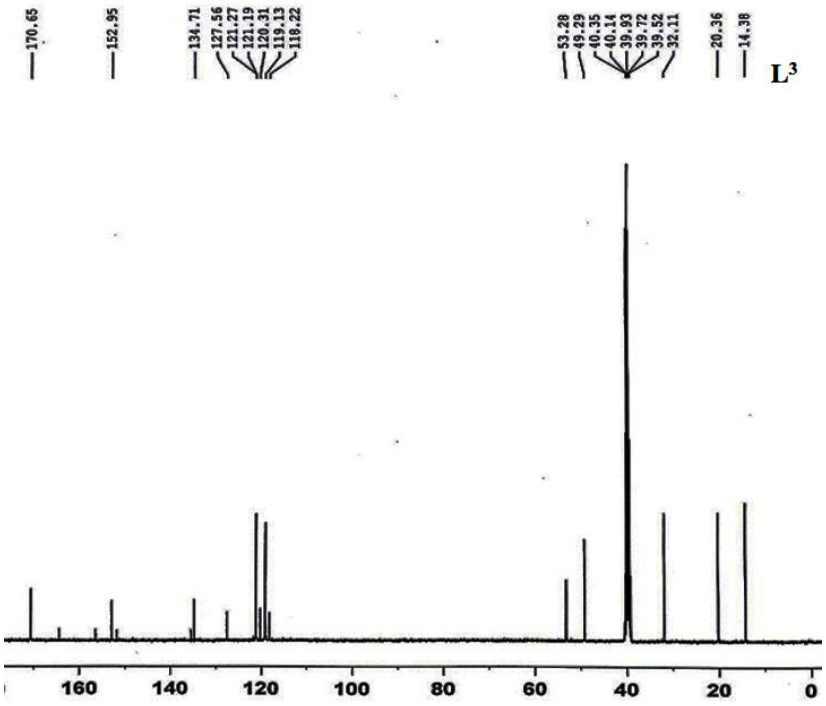

Annexure 25. ^{13}C NMR spectrum of **(L^3)**

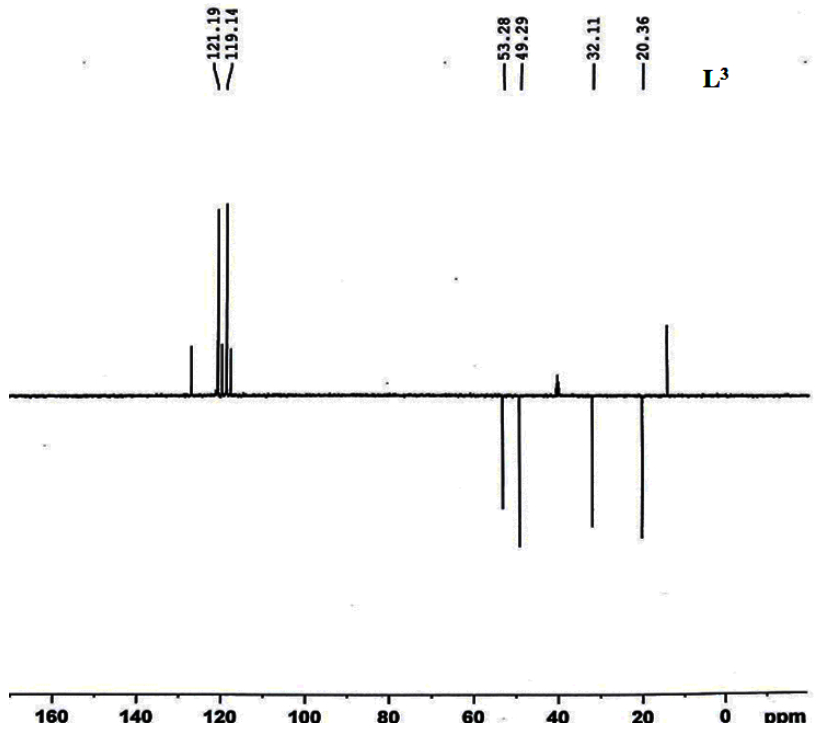

Annexure 26. DEPT-135 spectrum of **(L^3)**

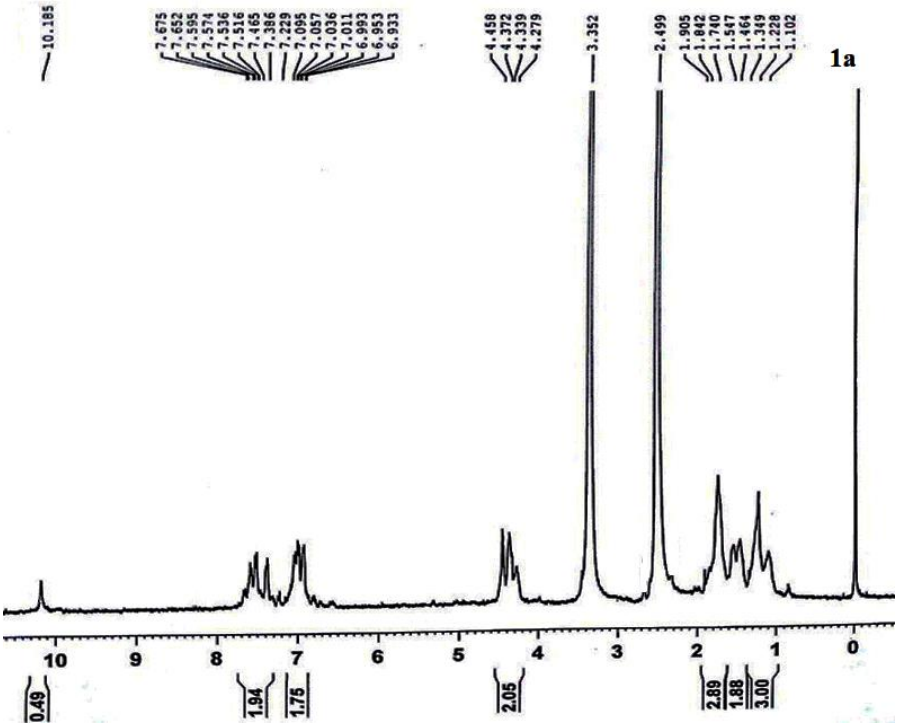

Annexure 27. ^{1}H NMR spectrum of **(1a)**

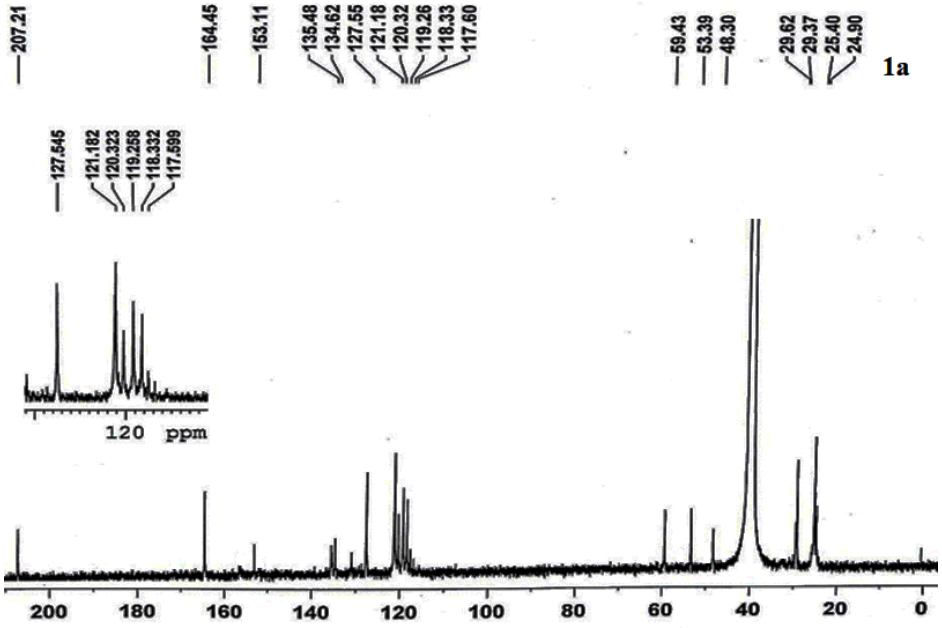

Annexure 28. ^{13}C NMR spectrum of **(1a)**

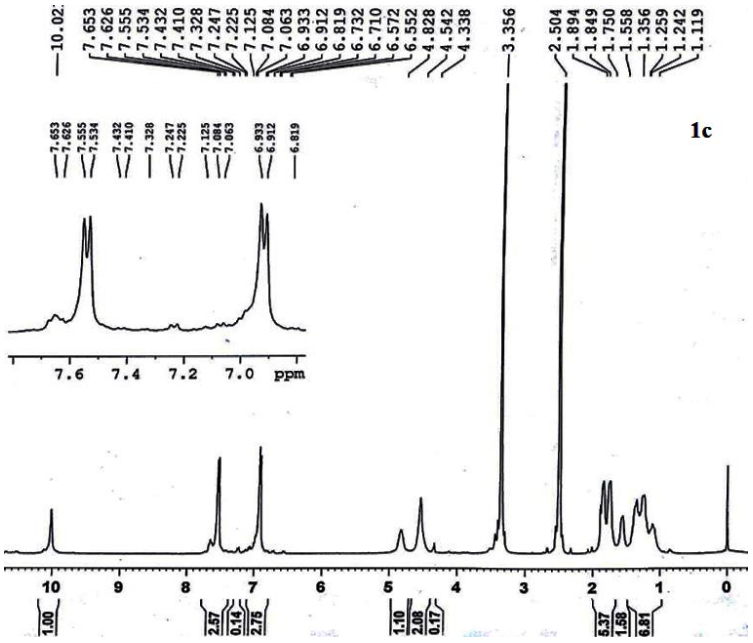

Annexure 29. ^{1}H NMR spectrum of **(1c)**

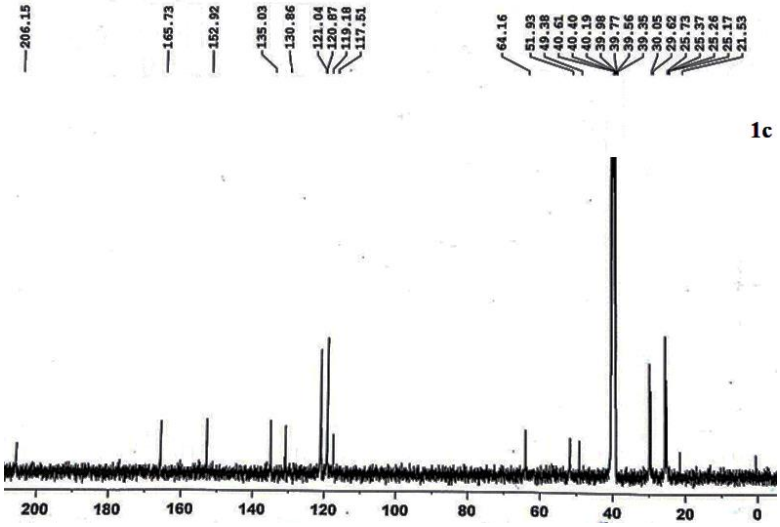

Annexure 30. ^{13}C NMR spectrum of **(1c)**

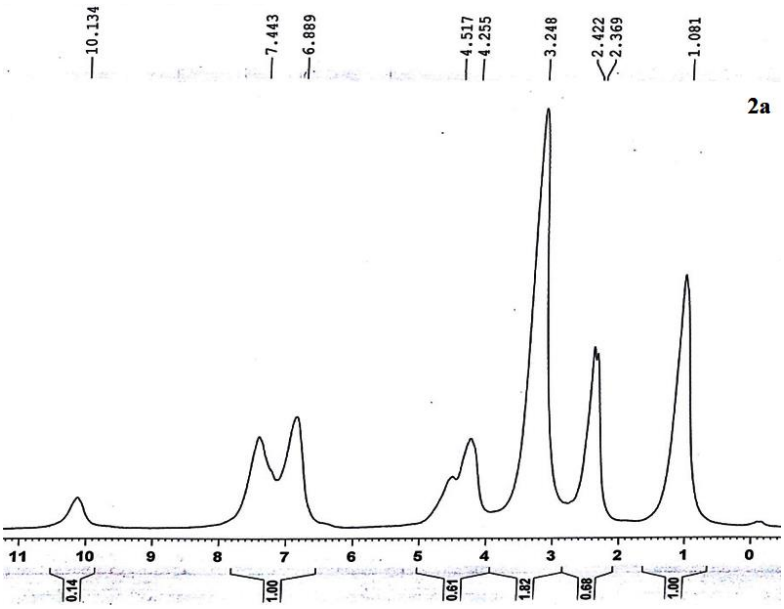

Annexure 31. ^{1}H NMR spectrum of **(2a)**

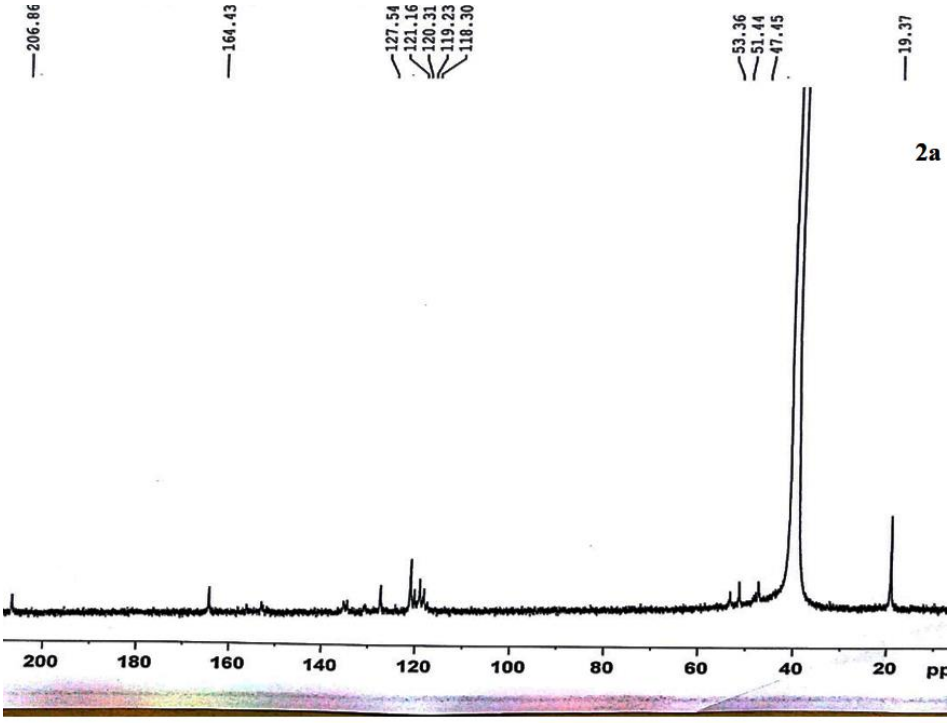

Annexure 32. ^{13}C NMR spectrum of **(2a)**

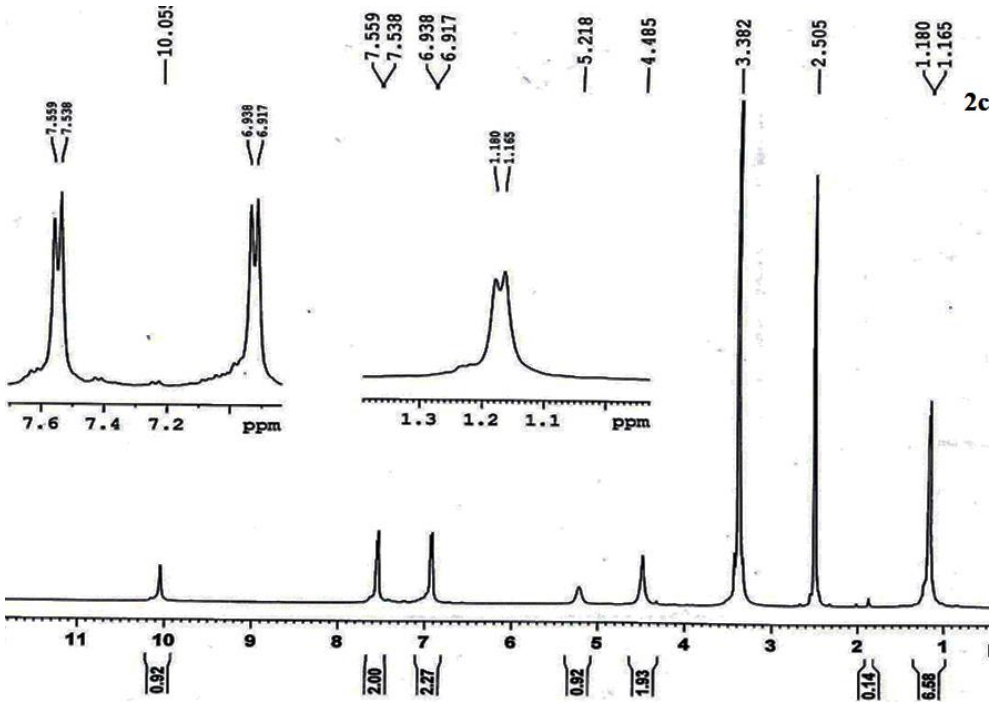

Annexure 33. ^{1}H NMR spectrum of **(2c)**

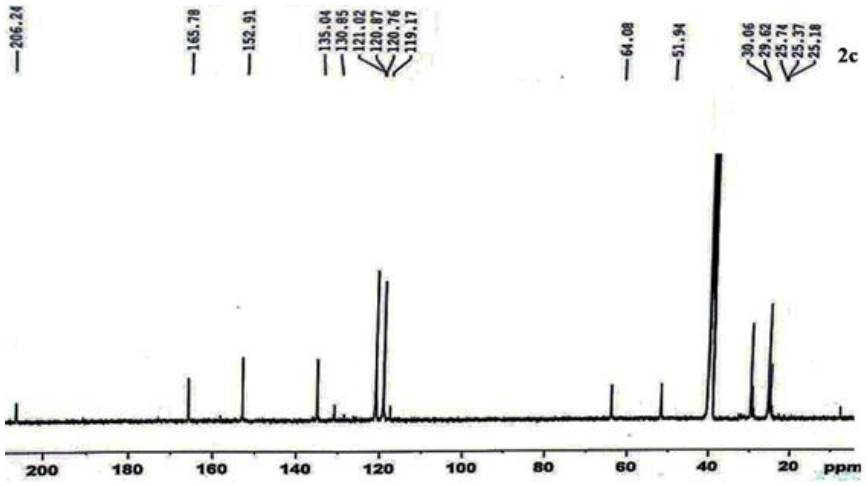

Annexure 34. ^{13}C NMR spectrum of **(2c)**

Fluorescence Study

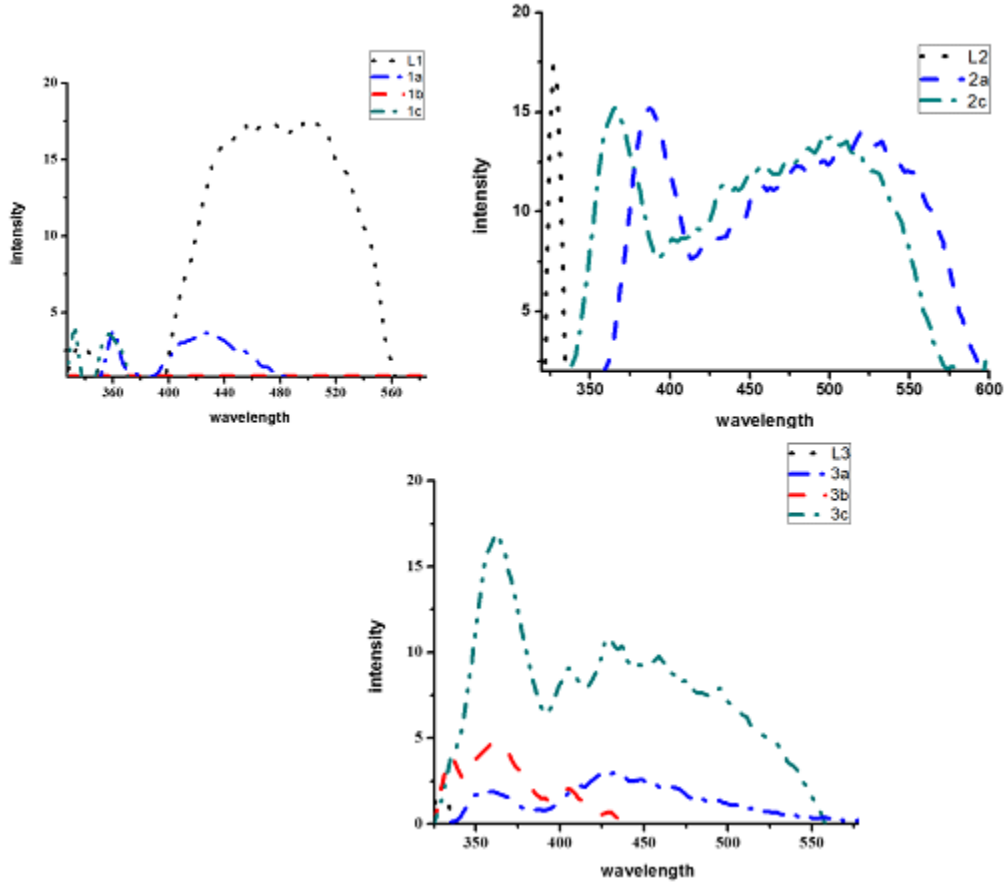

Annexure 35. Fluoresecence emmission spectra of **L^1 @** λ_{ex}= 305 nm, **1a @** λ_{ex}= 326 **and 1c @** λ_{ex}= 302 nm;(b) **L^2 @** λ_{ex}= 301 nm**, 2a @** λ_{ex}= 325 nm**,** and **2c @** λ_{ex}= 302 nm;(b) **L^3 @** λ_{ex}= 303 nm, **3a @** λ_{ex}= 321 nm**, 3b @** λ_{ex}= 303 nmand **3c @** λ_{ex}= 302 nm in DMF solution.

5.6.2 Thermogravimetric study

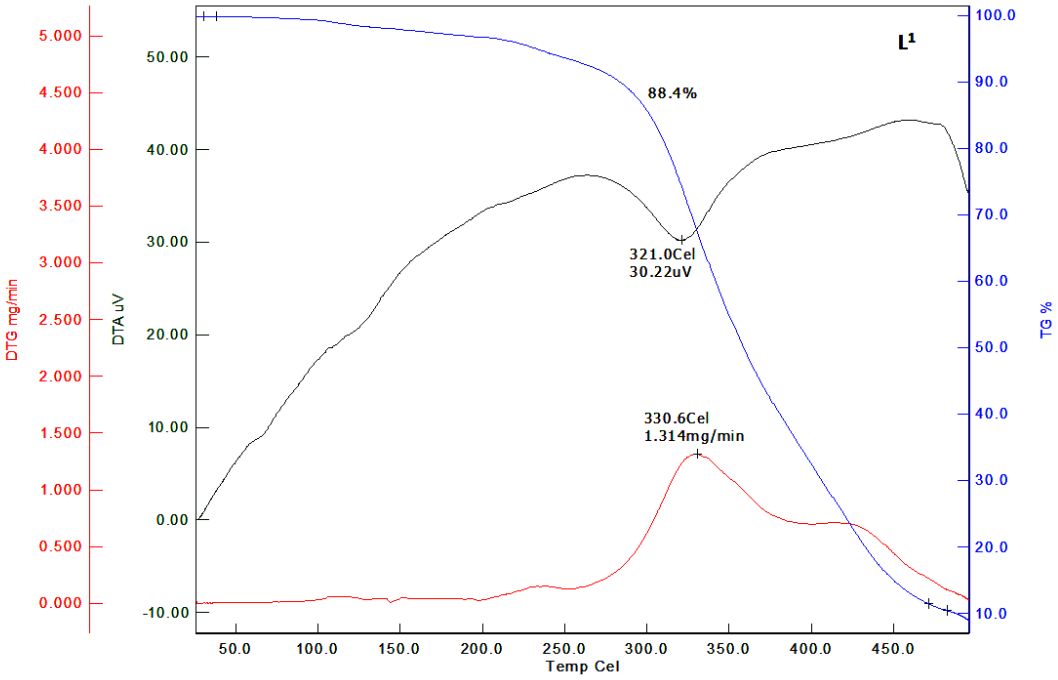

Annexure 36. TGA/DTA plot compounds **L^1**.

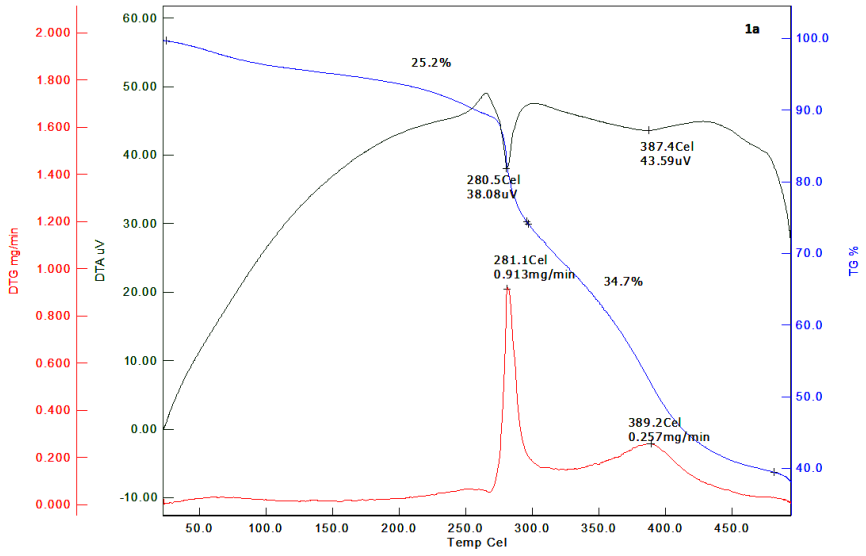

Annexure 37. TGA/DTA plot compounds **1a.**

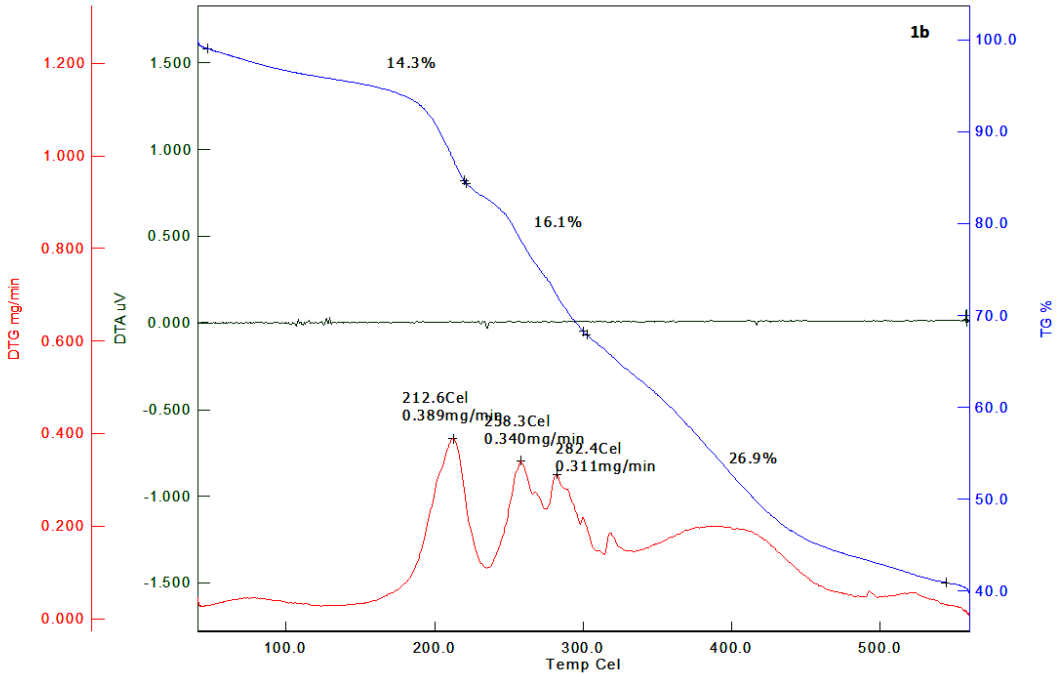

Annexure 38. TGA/DTA plot compounds **1b**.

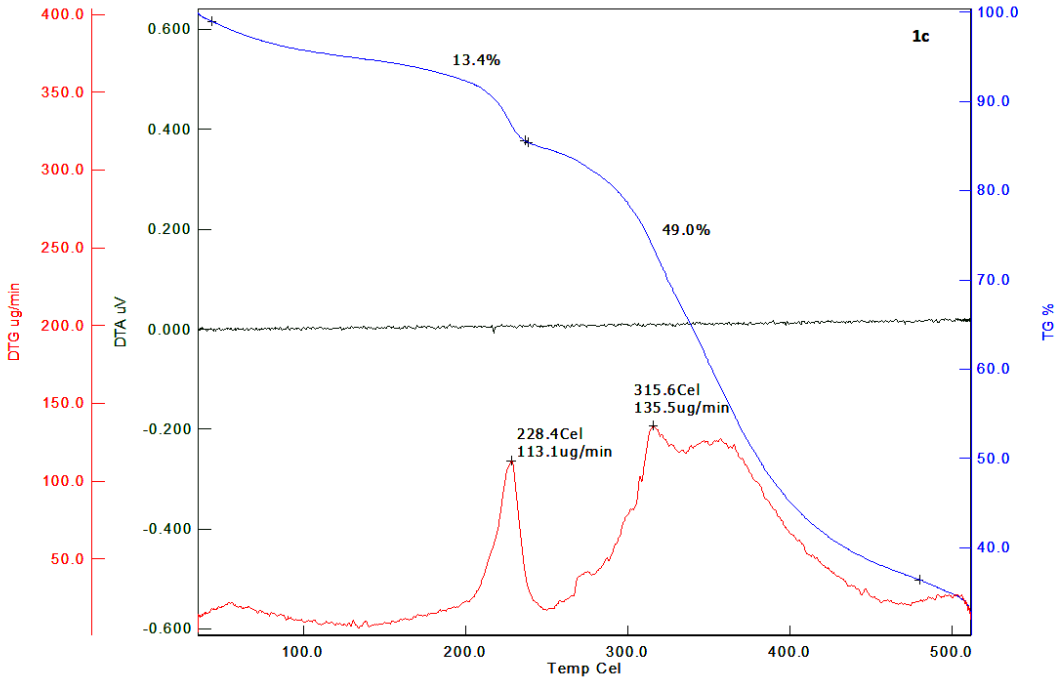

Annexure 39. TGA/DTA plot compounds **1c**.

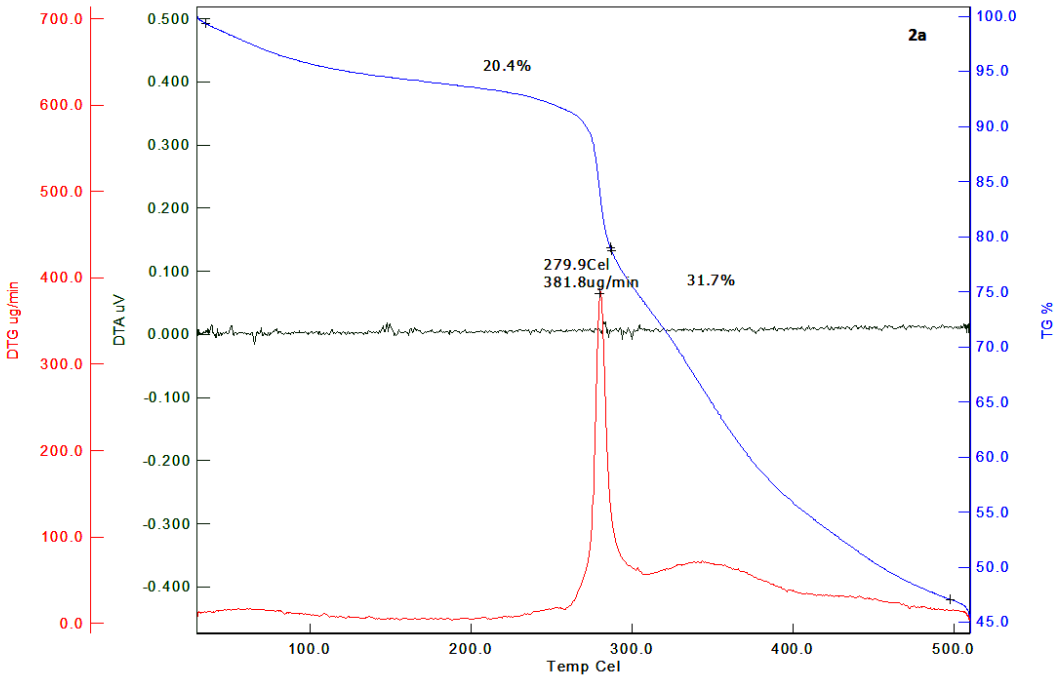

Annexure 40. TGA/DTA plot compounds **2a.**

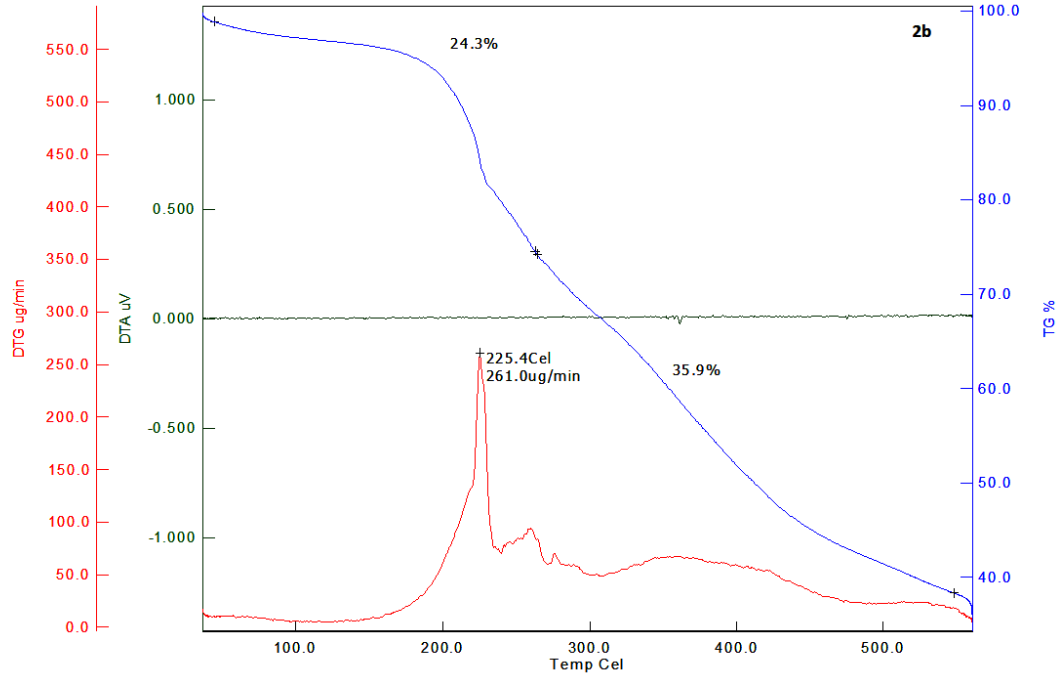

Annexure 41. TGA/DTA plot compounds **2b**.

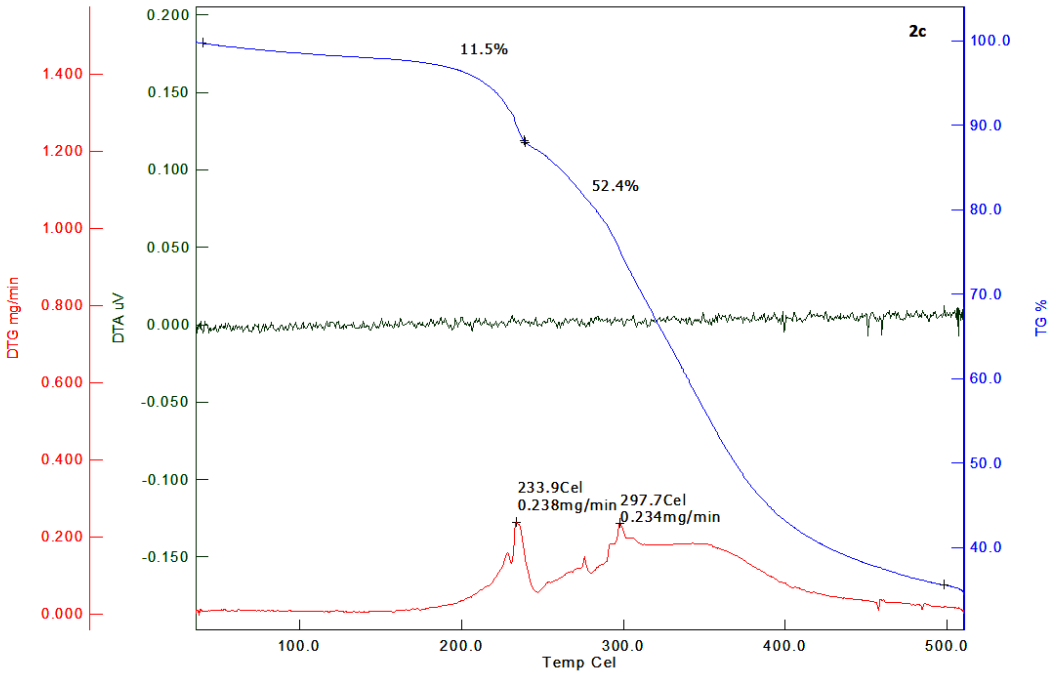

Annexure 42. TGA/DTA plot compounds **2c**.

This part of work is under communication: Manuscript ID: slct.201702296

The additional supporting Information related to this chapter is provided in the CD as follows:

Chapter 5

1. NMR Spectra: **Figure 1-5**
2. IR Spectra: **Figure 6-10**
3. Thermogravimetric analysis: **Figure 11-14 and Table 1**
4. Geometry Optimization: **Table 2-5**
5. In vitro cytotoxic study: **Table 6-7** and **figure 15-17**